Geophys. J. Int. (2002) **148,** 575–595

A physical-model study of the statistics of seismic waveform fluctuations in random heterogeneous media

C. Sivaji,[1]* O. Nishizawa,[1] G. Kitagawa[2] and Y. Fukushima[3]

[1] *National Institute of Advanced Industrial Science and Technology* 305-8567, *Central* 7, 1-1-1 *Higashi, Tsukuba Ibaraki, Japan.*
E-mail: epchan@ni.aist.go.jp
[2] *The Institute of Statistical Mathematics,* 4-6-7, *Minami-Azabu, Minato-ku, Tokyo* 106-8569, *Japan*
[3] *Dept. of Geophysics, Graduate School of Science, Tohoku University Aoba-ku, Sendai,* 980-8578, *Japan.*

Accepted 2001 September 10. Received 2001 September 5; in original form 2001 February 12

SUMMARY

Using laboratory-scale physical models, we studied seismic waveform fluctuation in 3-D heterogeneous media, and evaluated the effects of short-wavelength random heterogeneity on seismic waves. We made two series of experiments: (1) waves are excited by the same source signal and propagate through three kinds of granitic rocks with different scales of heterogeneity, and (2) waves are excited by different frequencies but propagating through the same rock. A compression-mode piezoelectric transducer was attached to one side of the block, and the waveforms were measured at a 10 mm radius circular array with a 2° spacing, located on the other side. 180 waveforms are obtained at equal source–receiver distances with an equal wave radiation from the source. The source signals are one- or two-cycle sine-wave pulse with 0.5 MHz for different heterogeneities, and 0.25, 0.5, 1 and 2 MHz for the same heterogeneity. Waveforms were recorded by using a system equipped with a laser Doppler vibrometer as a sensor of elastic waves. The rock heterogeneities were investigated as the 1-D velocity fluctuations obtained from the 2-D microstructure images of the rock. By applying the exponential autocorrelation function, heterogeneities in the three rocks are characterized by similar fluctuation intensities (7.9–9.3 per cent) but different scale lengths ranging from 0.22 to 0.92 mm. We calculated the spatial correlation of waveforms, the correlation between an averaged waveform and observed waveforms, the energy partition with respect to lapse time, and the statistical distributions of the waveform parameters: correlation coefficients, traveltimes of *P* wave, and the log values of the *P*-phase energy. Correlation of waveforms, energy partition and statistical parameters of waveforms are investigated as a function of the normalize scale parameter *ka*: the product of wave number and the characteristic scale length of heterogeneity. We found that waveform parameters change the trends at $ka \sim 0.2$–0.3. When *ka* exceeds 0.2–0.3, scattered waves become strong and waveforms become more complicated. This may indicate a transition from an equivalent homogeneous medium to a scattering medium for seismic waves propagating through random heterogeneous medium.

Key words: heterogeneous media, physical model, scattering, seismic wave caustics, wave propagation.

1 INTRODUCTION

Seismic waveforms fluctuate when propagating through heterogeneous media. It is convenient and useful to separate the heterogeneity of the earth's interior into two kinds of heterogeneities: the long-wavelength heterogeneity and the short-wavelength heterogeneity (Sato & Fehler 1998). When investigating structures of the Earth's interior by seismic methods, we regard the long-wavelength heterogeneity as a target heterogeneity, and the short-wavelength heterogeneity as a fluctuation of physical properties from the target heterogeneity. Changes of seismic waveforms caused by the long-wavelength heterogeneities are well understood in modern seismology, but those caused by the short-wavelength heterogeneities are not well-studied, especially for 3-D wave propagation.

* Now at: Department of Science and Technology, New Delhi, India.
E-mail: sivaji@alpha.nic.in

Short-wavelength heterogeneity is often referred to as random heterogeneity. Random heterogeneity generates incoherent scattered waves when seismic waves propagating through a heterogeneous medium. The scattered waves are overlapped with the source signal and complex waveforms are observed at the stations. We may be able to regard the scattered waves as noise in the observed waveforms. However, this noise is site dependent and is not same as the noise that randomly appears in the time-series. The scattered waves are signal-induced waves associated with the interaction between the source wave and the random heterogeneity. It is therefore important to study the relationship between them. Since scattered waves are incoherent and the heterogeneity is presumed random, the statistical properties of seismic wave fluctuation will relate to the statistical properties of the random heterogeneity.

The statistical parameters of waveform fluctuation can be obtained from the correlation coefficients of waveforms between observation points and the fluctuations of arrival times or of wave energy in corresponding phases. The correlation coefficients of the signal wave and observed wave and their distributions are used for describing the waveform fluctuation. Energy partition of scattered waves is also important. Statistics of waveform parameters in different heterogeneous media, or for different wave frequencies in the same heterogeneous medium, would yield a method of quantitative evaluation of the relationship between the waveform fluctuation and heterogeneities.

The correlation coefficient is a statistical measure of the waveform resemblance. When waveforms are obtained at two different observation stations, the resemblance of the two waveforms indicates the effect of random heterogeneity on seismic waves: resemblance becomes poor when the effect of heterogeneity is strong. Waveform correlation has been studied in many fields in seismology and physical acoustics (Pechmann & Kanamori 1982; Thorbjarnadottir & Pechmann 1987; Menke 1999; Menke *et al.* 1990; Pullammanappallil *et al.* 1997; Horike & Takeuchi 2000; Derode & Fink 1997, 1998).

The energy of seismic waves decays with lapse time because of intrinsic attenuation and scattering. Seismologists study the relationship between energy partition with lapse time (or attenuation) in seismic waves and the heterogeneity of the medium: (Knopoff & Hudson 1967; Aki & Chouet 1975; Sato 1984; Dubendorff & Menke 1986; Frankel & Wennerberg 1987; Varadan *et al.* 1989; Jannaud *et al.* 1991; Fehler *et al.* 1992; Hoshiba 1993; Yoshimoto *et al.* 1993; Menke *et al.* 1985, 1995; Korn 1990, 1997; Canas *et al.* 1998; Campillo & Margerin 1999; Parra *et al.* 1999).

The amplitude and traveltime fluctuations were also studied to delineate the heterogeneities in the medium (Aki, 1973; Flatte & Wu 1988; Lynnes & Lay 1990; Muller *et al.* 1992; Roth 1997; Hoshiba 2000; Sivaji *et al.* 2001; Spetzler *et al.* 2001; Spetzler & Snieder 2001).

One of the best ways to clarify the relationship between seismic waveform fluctuation and random heterogeneity is to conduct well-controlled experiments on seismic wave propagation. Since numerical simulation of seismic wave propagation is still difficult for 3-D random heterogeneities, laboratory-scale physical model experiments of elastic wave propagation are useful to understand seismic wave propagation in heterogeneous media. We conducted a series of physical model experiments that exactly measure full waveforms in random heterogeneous media whose fluctuation properties are already known. We employed a laser Doppler vibrometer (LDV), which provides very accurate waveforms over the entire lapse time. We revealed the intensity and the characteristic scale length of velocity fluctuations in granitic rocks by microstructure image analysis. We observed elastic waves propagating through different rock samples having different scales of heterogeneity, or through one rock sample with different wave frequencies from the source.

We examined the spatial coherency of elastic waves as a function of distance to understand the effect of scattering on seismic waves in different random media, or in the same random medium with different wave frequencies. We also examined the energy partition with respect to the lapse time for both observed and scattered waves. The fluctuation of the *P*-arrival times are studied by comparing statistical distributions of arrival times for different heterogeneous media. Statistical analysis is also employed for the spatial fluctuation of the *P*-wave energy. On the basis of those results, we quantify the effects of short-wavelength heterogeneity on seismic waves and discuss some significant effects of the short-wavelength heterogeneity on resolution of the conventional seismic imaging methods.

2 WAVEFORM MEASUREMENT

We employed different rock samples $30 \times 30 \times (8–9)$ cm as random heterogeneous media. A 5 mm diameter, disk-shaped piezoelectric transducer (PZT) with a 2 MHz compression-mode characteristic frequency was used as the source of elastic waves. This PZT was fixed at the centre of one of the 30×30 cm surfaces of the sample (Fig. 1). A wavelet with one or two cycles of sine waves was generated by a wave synthesizer and amplified to a 100 V peak-to-peak amplitude. The electric signal was transmitted to the PZT which generates elastic waves. A thin reflection sheet was glued on the opposite surface of the sample and an observation array was set up on this reflection sheet. The reflection sheet consists of small spherical glass lenses with diameter 50–60 μm. An optical unit of LDV is equipped with a tri-axial stage and its controller. The laser beam (He-Ne laser: wavelength $\lambda = 632.8$ nm) is moved and focused on the measuring point within a very small beam aperture; the same diameter of the glass lens or less. The positioning error of the beam is mostly within the diameters of the spherical lenses.

The Doppler shift of the laser beam reflected from the spherical lenses is measured as voltage signals and converted into the particle velocities of elastic waves. The beam direction is perpendicular to the surface and detects the velocity component of moving spherical lens (Nishizawa *et al.* 1998). Since the signal to noise ratio is very low, the waveform of each shot is stacked about 1000 times to obtain high quality data.

We observed 180 waveforms in a circular array with a 10-mm radius, and with a station spacing of 2°, or about 0.35 mm. This spacing is small enough to detect the phase correlation of elastic waves when compared to the wavelength of *P* and *S* waves; for example, in rock samples, wavelength is about 10 and 5–6 mm for 0.5 MHz *P* and *S* waves, respectively. Since the circular array is axisymmetric and the propagation distance for each observation point is equal, the geometrical spreading effect is the same for all waveforms. The effect of velocity anisotropy in granitic rocks (Sano *et al.* 1992) will be negligible when comparing waveforms in the array because the radiation angle deviates from the normal of the PZT by only 6–7°. The compression-mode PZT also provides axisymmetric radiation patterns for the *P* and *SV* wave (Fukushima 2000). Then all

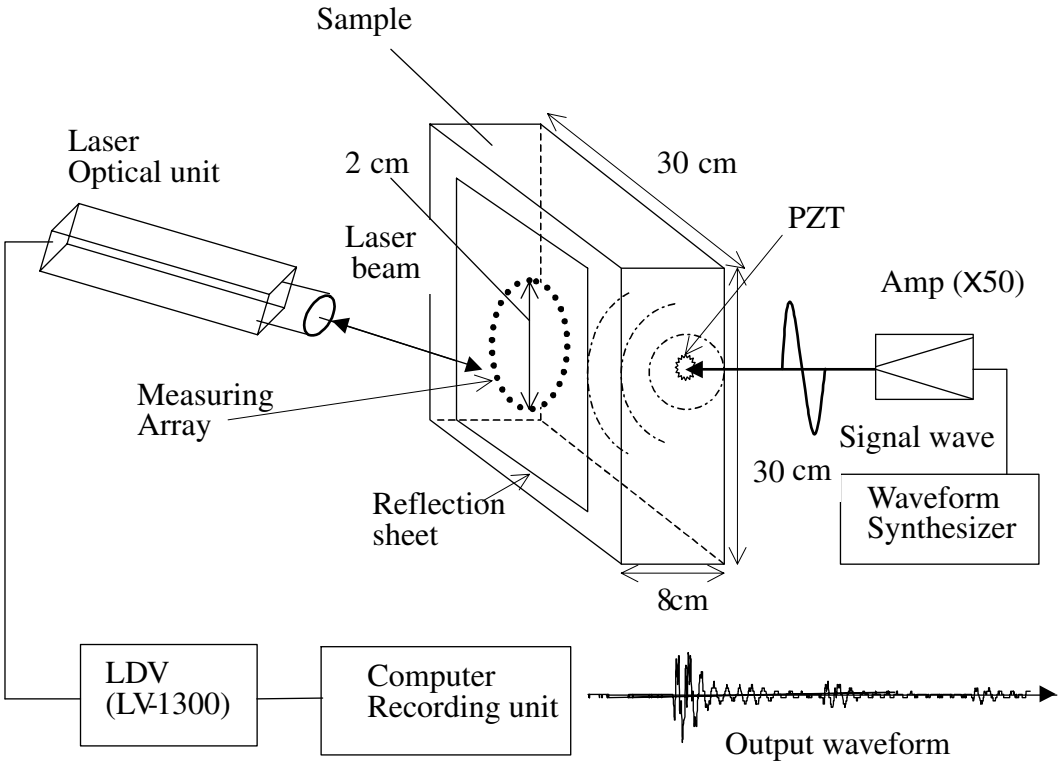

Figure 1. An illustration of physical model experiment. The elastic wave is generated from a piezoelectric transducer (PZT) attached at one of the major surfaces of the sample and received at the opposite surface. Waveforms are measured over a circular array of 2 cm diameter at every 2° with its centre coinciding with the symmetric axis of the disk-shaped PZT.

waveforms in the array should show high resemblance when the medium is homogeneous. This source–receiver configuration is ideal for studying the spatial coherency between the waveforms because observed differences in the waveforms are uniquely attributed to the heterogeneities embedded around the ray paths.

We measured waveforms for steel, Westerly, Oshima and Inada granites with a constant source frequency of 0.5 MHz. Waveforms of the three granitic rocks are shown in Fig. 2. Steel is used as a reference of complete homogeneous medium. For the Westerly granite, we measured the waveforms with different source frequencies of 0.25, 0.5, 1 and 2 MHz to understand the effect of frequency on the waveform fluctuation.

3 STATISTICAL BACK GROUND

3.1 Coherent and scattered wave fields

We employ an ensemble average to decompose the observed waveform into coherent and incoherent parts, which describe the average and the random fluctuations of physical properties in the medium, respectively. The observed waves can be regarded as fluctuated waves consisting of a coherent wave superimposed by the scattered waves.

The observed waveform at the ith station at time t can be written as a combination of coherent and incoherent waveforms. The coherent waveform represents the wave propagating through an equivalent homogeneous medium with an averaged physical property of the medium and the incoherent waveform represents the fluctuations of the physical property in the medium (Ishimaru 1975; Kinney & Clay 1984). We define that the coherent wave is an ensemble average of all waves in the array.

$$w_i^{(\mathrm{o})}(t) = w^{(\mathrm{c})}(t) + w_i^{(\mathrm{s})}(t) = \frac{1}{N}\sum_{i=1}^{N} w_i^{(\mathrm{o})}(t) + w_i^{(\mathrm{s})}(t)\,, \tag{1}$$

where $w_i^{(\mathrm{o})}(t)$ and $w_i^{(\mathrm{s})}(t)$ are the observed wave and the incoherent wave at the ith station, respectively, and $w^{(\mathrm{c})}(t)$ is the coherent wave defined as an averaged waveform for the all N observation points. The incoherent wave is hereafter referred to as the scattered wave. The importance of separating the coherent and the scattered waves from the observed wave for elucidating elastic wave attenuation in random media was discussed by Varadan *et al.* (1989), and more recently by Horike & Takeuchi (2000).

3.2 Spatial coherency

The waveform consists of the *P*-, *S*- and the two-fold reflected phases $PP'P''$ followed by their respective coda (Fig. 3). The *S* waves are not strong because the array is in the direction close to the node of the *SV*-wave radiation from a compression source (Fukushima 2000; Tang *et al.* 1994). Those three phases are discernible for the experiments of 0.5 MHz steel and 0.25 MHz Westerly granite (Figs 3, 4). However, in 0.5 MHz

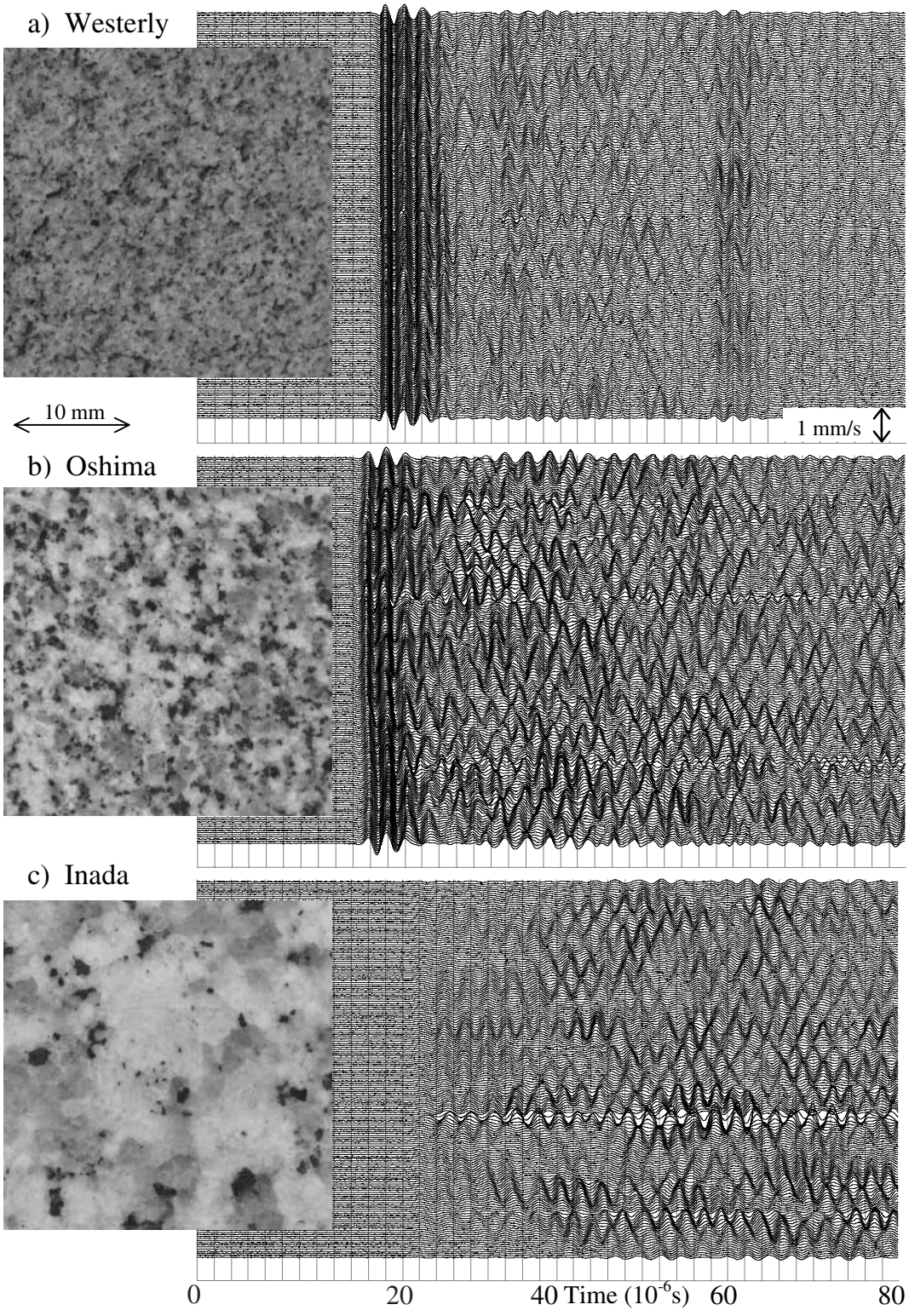

Figure 2. The microstructure of the three granitic rocks and the corresponding 180 waveforms observed over the circular array. The scales of microstructure images and the velocity are shown.

Oshima and 2 MHz Westerly, the *S* and *PP′P″* are not clear (Figs 3, 4). To clarify the effect of random heterogeneity on waveform fluctuation, we calculate the correlation coefficients of those phases with respect to the space lag between stations in the circular array. We selected three different time windows containing *P*, *S* and *PP′P″*. When *S* and *PP′P″* are unclear, we select the time window based on the traveltimes of those phases.

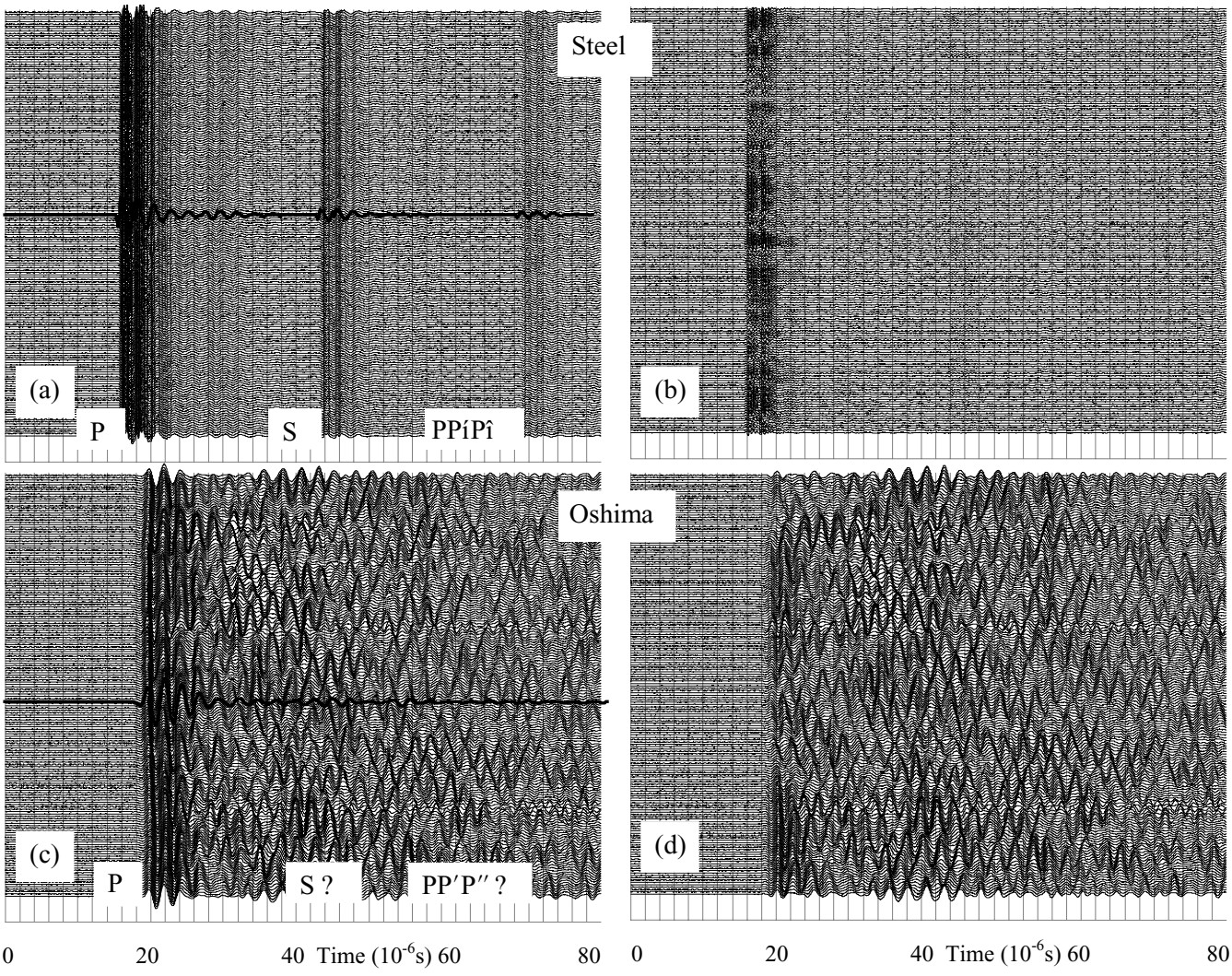

Figure 3. Observed and scattered waveforms for steel (a) & (b) and Oshima (c) & (d). The coherent wave is shown with the thick line. The *P*, *S* and *PP′P″* phases are identified in the coherent wave. The scattered wave field is obtained by removing coherent wave part from (a). *S* and *PP′P″* phases in Oshima cannot be identified.

The correlation coefficient $C_L(ij)$ between the array elements i and j of corresponding phases of the observed wave is

$$C_L(ij) = \frac{\int_{T_s}^{T_e} [w_i^{(o)}(t) - \overline{w}_i^{(o)}(t)][w_j^{(o)}(t) - \overline{w}_j^{(o)}(t)]dt}{\sqrt{\int_{T_s}^{T_e} [w_i^{(o)}(t) - \overline{w}_i^{(o)}(t)]^2 dt} \sqrt{\int_{T_s}^{T_e} [w_j^{(o)}(t) - \overline{w}_j^{(o)}(t)]^2 dt}} \quad (2)$$

where T_s and T_e represent the starting and ending times of the time window, and $\overline{w}_i^{(o)}$ represents the average of the observed wave in the time window between T_s and T_e:

$$\overline{w}_i^{(o)} = \frac{1}{T_e - T_s} \int_{T_s}^{T_e} w_i^{(o)}(t)dt. \quad (3)$$

The integral with respect to time can be replaced as a summation over T_s and T_e. $C_L(ij)$ is averaged for all pairs of (i, j) having the same distance between stations, $\overline{C}_L$. The change of $\overline{C}_L$ with respect to the station distance suggests a relationship between the fluctuations of seismic waves and heterogeneity.

3.3 Coherency between coherent waves and observed waves

Since the scattered wave is a signal-induced wave, it is related to the original signal that is actually unknown. We tentatively assume that the coherent wave defined by eq. (1) represents the signal in the equivalent homogeneous medium and compare the waveforms between the observed and coherent waves. The coherency between the observed wave and the coherent wave at each station of the array will be a measure of the wave fluctuation produced by heterogeneity. The correlation coefficient between coherent and observed wave at the ith station in the array is then calculated as

$$C_O(i) = \frac{\int_{T_s}^{T_e} [w_i^{(o)}(t) - \overline{w}_i^{(o)}][w^{(c)}(t) - \overline{w}^{(c)}]dt}{\sqrt{\int_{T_s}^{T_e} [w_i^{(o)}(t) - \overline{w}_i^{(o)}]^2 dt} \sqrt{\int_{T_s}^{T_e} [w^{(c)}(t) - \overline{w}^{(c)}]^2 dt}}, \quad (4)$$

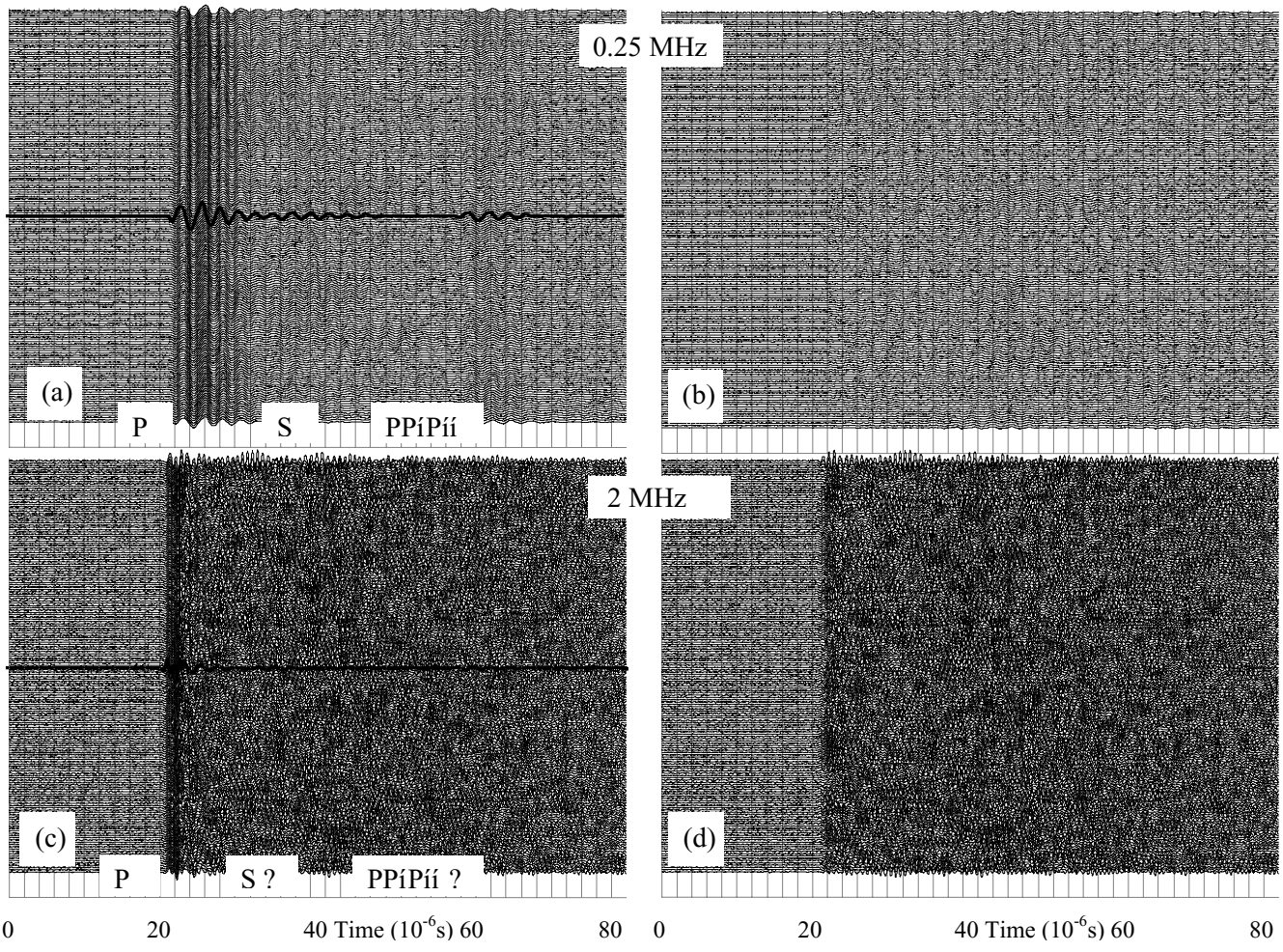

Figure 4. Observed (a and c) and scattered (b and d) waveforms for Westerly granite at different source frequencies 0.25 MHz and 2 MHz. The scattered waves are obtained by removing the coherent wave part (thick line) from the observed wave. The *S* and *PP'P''* phases are not clear even on the coherent wave for 2 MHz because of the predominance of scattered waves.

where $\overline{w}^{(c)}$ represents the average of the coherent wave in the time window between T_s and T_e:

$$\overline{w}^{(c)} = \frac{1}{T_e - T_s} \int_{T_s}^{T_e} w^{(c)}(t)dt\,. \tag{5}$$

We can estimate the random character of wave fluctuation by comparing the $C_O(i)$ at each station.

3.4 Energy partition with respect to lapse time

In the time domain, the energy of the direct wave can be expressed as a sum of the squared amplitudes in the window containing the direct arrival (Frankel & Wennerberg 1987; Korn 1997). We computed the wave energy in an appropriate time window by

$$E_i(t_m) = \int_{t_1}^{t_2} A_i^2(t)dt\,, \tag{6}$$

where $A_i(t)$ is the wave amplitude at the ith station at time t, and t_m is the central time (mid-point) of the window between t_1 and t_2. The energy estimated in each window is normalized by the total energy of the waveform starting from the *P*-wave onset to the end of the waveform. The total normalized energy of all waves in the array for each time window is computed as

$$\overline{E}(t_m) = \frac{\sum_{i=1}^{N} \int_{t_1}^{t_2} A_i^2(t)dt}{\sum_{i=1}^{N} \int_{t_P}^{T} A_i^2(t)dt}\,, \tag{7}$$

where t_P is the arrival time of *P* wave, and T is the total lapse time of the waveform. The normalized energy, $\overline{E}(t_m)$, is computed by shifting the window until the end of the waveform for observed and scattered waves. The variation of the normalized energy with lapse time is hereafter referred to as the energy partition pattern.

3.5 Spatial fluctuations of arrival times and energy of *P* waves

In the present experiments, observed waves are generated from a narrow wavelet and the time-series of observed wave is not stationary. However, if we properly divide the observed time-series into some short intervals, the short intervals are regarded

as locally stationary time-series (Kitagawa & Akaike 1978). We have adopted a method proposed by Takanami & Kitagawa (1991) for estimating the arrival time of the seismic wave. The technique involves the fitting of an optimum autoregressive (AR) model to the time-series, using the Akaike Information Criterion (AIC).

We divide the entire waveform into some short time-series from 1 to k. The jth interval contains N_j data points from $w(t_{n_{j0}})$ to $w(t_{n_{j1}})$, where $n_{j0}=\sum_{i=1}^{j-1}N_i+1$ and $n_{j1}=\sum_{i=1}^{j}N_i$. By using the autoregressive model, $w(t_n)$ is expressed as a linear combination of the previous values of the time-series, $w(t_{n-i})$, $i=1,2,\ldots,m_j$:

$$w(t_n)=\sum_{i=1}^{m_j} a_{ji}w(t_{n-i})+v_{nj} \tag{8}$$

where a_{ji} are the autoregressive coefficients of order m_j, and v_{nj} represents the Gaussian white noise sequence in the jth interval with zero mean and the variance σ_j^2. The autoregressive coefficients a_{ji} are estimated by minimizing the variance of the distribution v_n.

$$\sigma_j^2=\frac{1}{N}\sum_{n=n_{j0}}^{n_{j1}}\left(w(t_n)-\sum_{i=1}^{m_j}a_{ji}w(t_{n-i})\right)^2 \tag{9}$$

The highest probability of realization is given by the minimum value of the summation of σ_j^2.

$$\sum_{j=1}^{k}\sigma_j^2\rightarrow\text{minimum}$$

When estimating the AR coefficients, we have an ambiguity of determining the order of AR model, m_j. Increasing m_j provides a narrower distribution of v_{nj} and the realization probability becomes higher. However, this misleads estimation of AR coefficients because too great a decrease of σ_j^2 overestimates the probability of realization. A statistically sound trade-off between increasing m_j and decreasing σ_j^2 is obtained by calculating the following AIC value:

$$\mathrm{AIC}_j=(N-m_1)(\log 2\pi+1)+\sum_{j=1}^{k}N_j\log\sigma_j^2+\sum_{j=1}^{k}(m_j+1) \tag{10}$$

A smaller AIC indicates a better model for applying the locally stationary AR model.

A simple example is to divide the waveform into the initial noise part and the P-phase part. We select a proper length of the time-series data of the waveform including the P phase, and calculate AIC values by changing the dividing point of the time-series. We obtain a minimum-AIC point that divides the waveform into the initial noise part and the signal part. Then the point represents the onset time of the direct P phase.

Sivaji *et al.* (2001) examined the reliability of picking the first arrival of P wave. The waveform and AIC values are shown in Fig. 5. The AIC values are calculated by changing the dividing point between the initial noise part and the P-wave part. The lower figure shows that the minimum AIC appears at the point number 447, which corresponds to the onset of the P wave, an arrival time. We obtained the arrival times of the P-waves for all array stations.

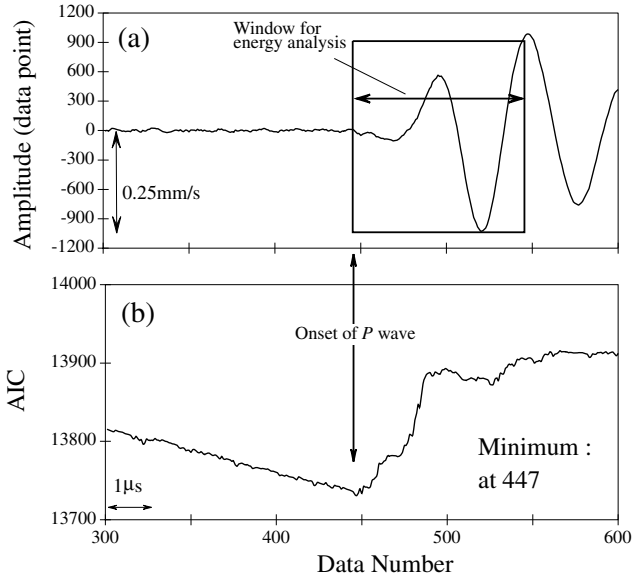

Figure 5. An example of arrival time determination by time series analysis. (a) an observed waveform and (b) AIC values associated with the waveform. The AIC minimum value at the data number 447 corresponds to the onset of the P-wave. The rectangle in (a) indicates a window for calculating the P-wave energy.

4 RESULTS

4.1 Random medium analysis

To study the quantitative relationships between waveform fluctuation and heterogeneity, it is essential to quantify the heterogeneity of the medium prior to the analysis of the waveform data. Since there are no large heterogeneities such as xenoliths, large-scale porphylitic structure, or large crystals in the granitic rocks used for these experiments, the rocks are considered to be homogeneous in the long-wavelength but heterogeneous in the wavelength of ultrasonic wave. The fluctuation can be described by the spatial autocorrelation function (ACF) approximated by Gaussian, exponential or von Kárman type function with the characteristic parameters of the medium: the intensity of fluctuation, the characteristic scale-length parameter of the heterogeneity, and if necessary, the characteristic constants in the ACF (Frankel & Clayton 1986; Sato & Fehler 1998). In the following, we present a method to estimate the intensity and scale length of velocity (or slowness) fluctuation.

The granite samples consist of three prominent minerals: biotite, quartz and plagioclase. Microstructure images of the granitic rocks are obtained with 600-dpi (dot per inch) colour data. The colour images are converted to tri-colour images to identify the three minerals: white, gray and black colour corresponding to plagioclase, quartz and biotite, respectively. The 1-D mineral distribution maps are obtained by traversing the image. The maps are then converted to P-velocity maps by assigning velocity values to the minerals (Fukushima 2000; Spetzler *et al.* 2001). When assigning mineral velocities, we assume random orientations of minerals and take the velocity anisotropy of biotite into account because biotite shows strong velocity anisotropy (Aleksandrov & Ryzhova 1961). The anisotropy of biotite is the major part of the velocity fluctuation in granitic rocks.

Rocks contain cracks that affect seismic wave velocity. The porosities of the three granitic rocks are 0.5–1 per cent mostly contained in thin cracks. Oshima granite shows a considerable velocity anisotropy due to preferred orientation of cracks (Sano *et al.* 1992). However, the measurements of waveforms in different directions suggest that the effect of cracks on observed waveforms is not strong for frequencies less than 1 MHz (Nishizawa *et al.* 1997; Fukushima 2000). Most cracks in granitic rocks exist in crystals or at crystal boundaries, and the crack size is strongly related to the grain size of the rock forming minerals. Therefore, if cracks affect the rock heterogeneity, the effect of cracks on heterogeneity is considered to be similar to that of velocity fluctuation due to the velocity contrast of the minerals, or the effect will be an additional fluctuation at the high-frequency portion of the spectral density because of the thin and flat shape of cracks. Here, we neglect the crack effect when describing the heterogeneity of granitic rocks.

To calculate ACF from discrete velocity distribution, we used a method based on Holliger & Levander (1992, 1994), where they obtained ACF from geologic maps. We calculate the Fourier spectral density for the velocity fluctuation and then obtain ACF by inverse Fourier transform. Details of the analysis are described in Spetzler *et al.* (2001).

The average power spectra of 20 traverse lines and the corresponding ACFs for the Westerly, Oshima and Inada granites are shown in Figs 6(a)–(f). The estimated ACFs (Figs 6d–f, solid line) have been fitted to the exponential ACF given by

$$F(x) = \varepsilon^2 \exp\left(-\frac{x}{a}\right), \tag{11}$$

where ε is the standard deviation of velocity (slowness) fluctuation, a is the correlation length, and x is the spatial lag. The best-fit exponential-type ACF is shown with a dashed line in the corresponding correlation plots (Figs 6d–f). The estimated intensity ε and characteristic scale length a of three different granitic rocks are given in Table 1. The values of ε and a are 8.5 per cent, 0.22 mm; 9.3 per cent, 0.46 mm; and 7.9 per cent, 0.92 mm for Westerly, Oshima and Inada, respectively. The intensity of velocity fluctuation, ε, shows a small variation. The heterogeneities of the three granitic rocks are characterized by the exponential ACFs with similar intensity but different characteristic scale lengths.

The random medium analysis provides the relationships between frequencies of elastic waves as shown in Table 2. In the Table, measured *P*- and *S*-velocities are shown together with wavelength λ, wave number k, and ka, the product of the wavelength and the characteristic scale length of heterogeneity. The values of ε and a are not the same values for the *P*- and *S*-wave fluctuations. In granitic rocks, ε for *S* wave is larger than that for *P* wave because of the unique velocity anisotropy in biotite (Aleksandrov & Ryzhova 1961) but a shows similar

Table 1. Parameters of autocorrelation function. The scale length of heterogeneity a and the standard deviation of slowness fluctuations of three granitic rocks ε.

Rock	Scale length of heterogeneity a (mm)	Standard deviation of slowness fluctuation ε (per cent)
Westerly	0.22	8.5
Oshima	0.46	9.3
Inada	0.92	7.9

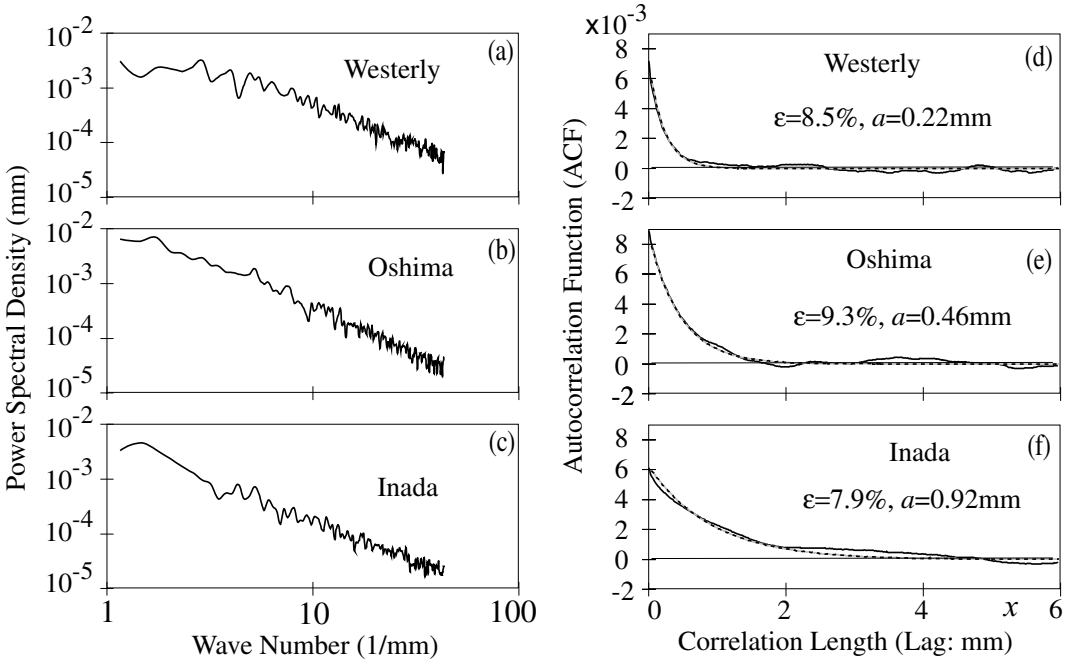

Figure 6. Power spectrum and autocorrelation function of 1-D velocity fluctuations for Westerly (a) & (d), Oshima (b) & (e) and Inada granites (c) & (f). ε and a indicate the standard deviation of velocity fluctuation and the characteristic scale length of heterogeneity. The best-fit exponential autocorrelation function is shown by dashed line.

Table 2. *P*- and *S*-wave velocities of granitic rocks, source frequencies, wavelength, wave number and *ka* values of the present experiments. *P*-velocities are measured values of the present source-receiver arrangement. (*Oshima shows strong anisotropy. The *S*-velocity is a range given by Sano *et al.* (1992)).

Rock	frequency MHz	*P*-wave				*S*-wave			
		velocity km/s	λ mm	k (mm^{-1})	ka	velocity km/s	λ mm	k (mm^{-1})	ka
Westerly	0.25	4.78	19.1	0.33	0.07	2.84	11.3	0.55	0.12
	0.5		9.6	0.66	0.14		5.7	1.11	0.24
	1		4.8	1.31	0.28		2.8	2.22	0.49
	2		2.4	2.63	0.56		1.4	4.43	0.97
Oshima	0.5	4.81	9.6	0.65	0.30	2.56–3.0*	6.0-5.1	1.23-1.05	0.56-0.48
Inada	0.5	3.78	7.6	0.83	0.76	2.53	5.1	1.24	1.14

values for the *P*- and *S*-wave fluctuations (Fukushima 2000). For calculating *ka* for *S* wave, we tentatively assume that *a* is same as that of *P* waves for the three granitic rocks.

4.2 Spatial coherency of waveforms

An example of the coherent and scattered waves is shown in Fig. 3 for steel and Oshima. The scattered waves for steel (Fig. 3b) are weak as expected from a homogeneous medium. The waveform in steel contains overtone modes of the source-transducer vibration. The overtone modes are high frequency and sensitive to the correlation coefficient. In steel, most of the incoherent waves are the overtone modes included in the *P* phase. However, the overtone modes disappear in rocks and do not affect the relationship between waveform and heterogeneity. The later $PP'P''$ phase is clear in steel. On the other hand, the scattered field in Oshima granite is predominant. The later phases like $PP'P''$ are masked by the scattered waves (Fig. 3c). A similar relationship between coherent and scattered waves is seen in the waveforms obtained for Westerly with different source frequencies: 0.25 and 2 MHz (Fig. 4). The coherent wave of 0.25 MHz source is stronger than that of 2 MHz source. The corresponding scattered wave of 0.25 MHz is very weak (Fig. 4b). On the other hand, the scattered waves for 2 MHz are predominant, suggesting strong scattering (Fig. 4d).

In order to understand the effect of heterogeneity on spatial coherency of waveform, an average of $C_L(ij)$ for all pairs of i and j with equal array separation, $\overline{C}_L$, is plotted against the distance. Fig. 7 shows $\overline{C}_L$ against distance for *P*, *S* and $PP'P''$ phases. The horizontal axis is the arc length of the array between two stations, i and j. The length of the arc is different from the actual distance between the array stations. However, the plots are only up to about $\pi/6$ radian of the arc. The difference between actual distance and the arc length is very small. Thus Fig. 7 represents the change of $\overline{C}_L$ against distance for different heterogeneous media or for different frequencies.

Figs. 7(a–d), show the spatial correlation for steel, Westerly, Oshima and Inada granites, respectively. The spatial coherency for *P*, *S* and $PP'P''$ phases exhibit distinctly different decay characteristics for steel and the three granitic rock samples. The $\overline{C}_L$ of *P*, *S* and $PP'P''$ phases decrease and converge on constant values at some critical distances, and oscillates around the constant values. The convergence value of $\overline{C}_L$ and the critical distance are different in different heterogeneities. $\overline{C}_L$ for *P* phase decreases to 0.84 in steel and 0.83 in Westerly at almost same critical distance 9 mm (Figs 7a,b). On the other hand, the convergence values of Oshima and Inada are smaller and the critical distance is shorter: 0.65 and 4 mm for Oshima and 0.1 and 3 mm for Inada, respectively (Figs 7c,d). The convergence values of $\overline{C}_L$ for *S* and $PP'P''$ phases are equal or smaller than *P* phases. In Oshima and Inada, the convergence values of $\overline{C}_L$ for *S* and $PP'P''$ phases are zero, and $\overline{C}_L$ of Inada oscillates between positive and negative values suggesting reverse phases.

The $\overline{C}_L$ for the different source frequencies are shown in Figs 7(e–h). The convergence values of $\overline{C}_L$ for *P*-wave are 0.85 and 0.84 for 0.25 and 0.5 MHz, respectively, at the critical distance of 9 mm. Whereas the *P*-wave coherency decreases sharply for the 1 and 2 MHz source frequency: the convergence values and the critical distances are 0.81 and 1.4 mm for 1 MHz, 0.67 and 1.0 mm for 2 MHz. $\overline{C}_L$ of the *S* and $PP'P''$ phases decreases gradually for 0.25 and 0.5 MHz with convergence values and the critical distances 0.7–0.8 and 6 mm for *S* and $PP'P''$ at 0.25 MHz, and 0.7 and 2.5 mm for the $PP'P''$ and 0.45 and 4 mm for the *S* of 0.5 MHz. For higher source frequencies, the convergence values become much smaller and the critical distances become much shorter: 0.3 and 1mm for the $PP'P''$, 0.1 and 1 mm for the *S* in 1 MHz, and almost zero and 1 mm for both *S* and $PP'P''$ in 2 MHz. Waveform resemblance becomes poor when the characteristic scale length increases or when the source wave frequency increases.

4.3 Coherency between coherent wave and observed waves

When the wave is fluctuated strongly by scattered wave, the correlation between the coherent wave and the observed wave becomes weak. The correlation between these two waves can be another measure for characterizing the complexity of wave field in a heterogeneous medium. $C_O(i)$ are plotted against the trace number of the array for steel, Westerly, Oshima and Inada granite (Fig. 8a) and for different source frequencies in Westerly granite (Fig. 8b). The averages of $C_O(i)$ and $\overline{C}_O$ decrease in the following order of steel (0.97), Westerly (0.94), Oshima (0.63) and Inada (0.23). For different frequencies, the $\overline{C}_O$ decreases from 0.96, 0.94, 0.74 and to 0.49 with increasing frequency from 0.25, 0.5, 1 and to 2 MHz, respectively.

This indicate that the fluctuation of $C_O(i)$ increases with decreasing its average $\overline{C}_O$. The probability density of $C_O(i)$ is shown in Fig. 9 for each experiment. The mean and the standard deviation of the distribution of $C_O(i)$ ($\overline{C}_O$ and σ_C, respectively) are listed in Tables 3 and 4 together with other parameters.

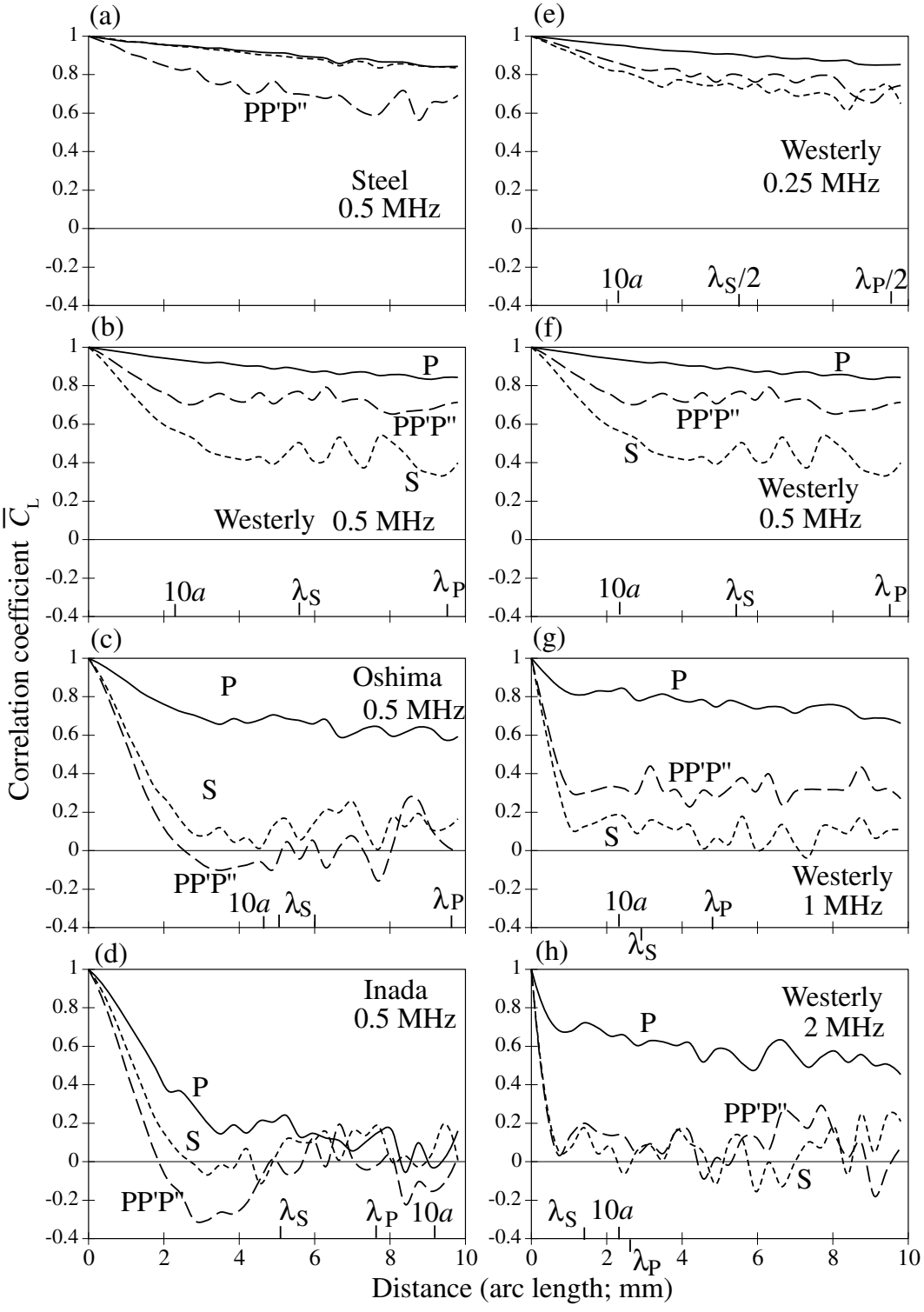

Figure 7. Average cross correlation coefficient $\overline{C}_L$ of *P*, *S* and *PP′P″* phases. Correlation coefficients are plotted against arc length between stations: different heterogeneous media, (a) steel, (b) Westerly, (c) Oshima and (d) Inada for 0.5 MHz source frequency; and different source frequencies, (e) 0.25 (f) 0.5, (g) 1, (h) 2 MHz for Westerly granite. $\overline{C}_L$ for *P*, *S* and *PP′P″* phases are plotted by solid, dotted and dashed lines, respectively.

4.4 Energy partition in different media and different frequencies

Since the scattered wave is a signal-induced wave, the energy partition of the scattered wave against the lapse time should have some relationships to the energy partition of the observed wave. It is therefore interesting to compare the energy partition patterns against the lapse time between those two waves. The comparison will give some clues to understand mechanisms of scattered-wave excitation and waveform fluctuation from the original waveform. The temporal distribution of wave energy is shown in Fig. 10 for the three granitic rocks, and in Fig. 11 for

Table 3. Statistics of waveform fluctuation for three rocks. Scale length of heterogeneity, a; product of the scale length and the wave number, ka; average of the correlation coefficient between coherent and observed waves, $\overline{C}_O$; standard deviation of the correlation coefficient between coherent and observed waves, σ_C; standard deviation of arrival time fluctuation, σ_T; and standard deviation of log-energy fluctuation, σ_E. Steel provides parameters in complete homogeneous medium, showing errors of measurements. Source signal is a 0.5 MHz single cycle sine wave.

Medium	a (mm)	ka	$\overline{C}_O$	σ_C	σ_T (μs)	σ_E (arbitrary scale)
steel	–	0	0.97	0.02	0.23	0.06
Westerly	0.22	0.14	0.94	0.02	0.52	0.13
Oshima	0.46	0.30	0.63	0.08	0.70	0.32
Inada	0.92	0.76	0.23	0.19	2.20	0.84

different source frequencies. The plotted values are the wave energy in the unit time interval normalized by the total energy of the observed wave, and averaged over all array stations.

Since steel is homogeneous, the scattered energy after the direct P phase indicates the mismatch of high frequency overtone mode. The overtone modes disappear in the rock sample and

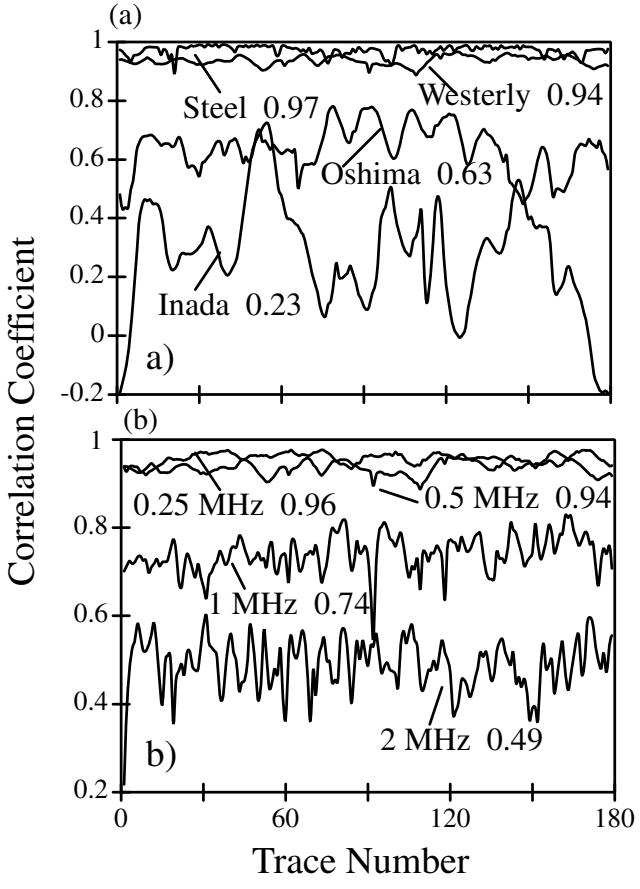

Figure 8. (a) The correlation coefficient between the coherent wave and the observed waves $C_O(i)$ for steel, Westerly, Oshima and Inada granites; (b) The correlation coefficient between the coherent wave and the observed waves for Westerly granites with different frequencies of 0.25, 0.5, 1, 2 MHz. Average values of correlation coefficients are shown in the figure.

Table 4. Statistics of waveform fluctuation for different wave frequencies in Westerly granite. Frequency of source sine wave, f; the product of the scale length and the wave number, ka; average of the correlation coefficient between coherent wave and observed wave, $\overline{C}_O$; standard deviation of the correlation coefficient between coherent wave and observed wave, σ_C; standard deviation of log-energy fluctuation, σ_E.

f (MHz)	ka	$\overline{C}_O$	σ_C	σ_E (arbitrary scale)
0.25	0.07	0.96	0.01	0.13
0.5	0.14	0.94	0.02	0.13
1.0	0.28	0.74	0.04	0.38
2.0	0.56	0.49	0.06	0.60

they have nothing to do with the present analysis. The scattered waves at the direct S phase and $PP'P''$ phase are very weak because of weak overtone modes in these phases (Fig. 3). The scattered wave in Westerly shows slightly larger background compared to steel and is almost uniformly distributed with respect to the lapse time. For both steel and Westerly, the major part of the wave energy concentrates in the P, S and $PP'P''$ phases.

On the other hand, Oshima and Inada show different partition patterns. In Oshima, the energy is mostly concentrated in P and S phases, but much energy is observed in the scattered-wave part. The energy partition of the scattered wave is not uniform over the lapse time, showing peaks around P, S and $PP'P''$ (not clear) phases. Considering that the scattered wave is a signal-induced wave, the scattered wave energy in Oshima after the S phase is larger than that expected from the direct S phase of the observed wave. This portion contains the scattered waves excited from the waves propagating in other directions. The compression source produces the maximum SV-wave energy at a radiation angle around 30° (Tang *et al.* 1994; Fukushima 2000), and the scattered waves after the S phase are produced by gathering the wave energy over the wide radiation angle from the source, suggesting the wide-angle scattering is strong in Oshima. The rapid decay of the scattered energy after the P phase may suggest that multiple scattering is not strong and only the forward scattering affects this portion. On the other hand, scattered-wave energy in Inada increases with the lapse time until about 60 μs, and then the energy gradually decreases. There is no remarkable energy concentration in the P, S and $PP'P''$ phases in Inada; the scattered waves strongly control the observed wave-energy partition against lapse time. This suggests that most of the wave energy is scattered and trapped in the medium, and then the scattered-wave energy gradually diffuses to the observation station.

Fukushima (2000) found that ε of the S-velocity fluctuation in Oshima is larger than that of P-velocity; 17%, almost twice of the P-velocity fluctuation. Considering that the ka for S wave is larger than the ka for P wave, the scattering intensity of S wave is much stronger than that of P wave. The scattering of S wave contains more multiple scattering than the scattering of P wave and causes the strong scattered energy after the S phase.

We also obtained similar energy partition for the different-frequency experiments in Westerly. P, S and $PP'P''$ phase are discernible in the observed energy partition for the 0.25 and 0.5 MHz source frequency. In the observed energy partition for 1 and 2 MHz source, only the P phase is discernible. For 0.25

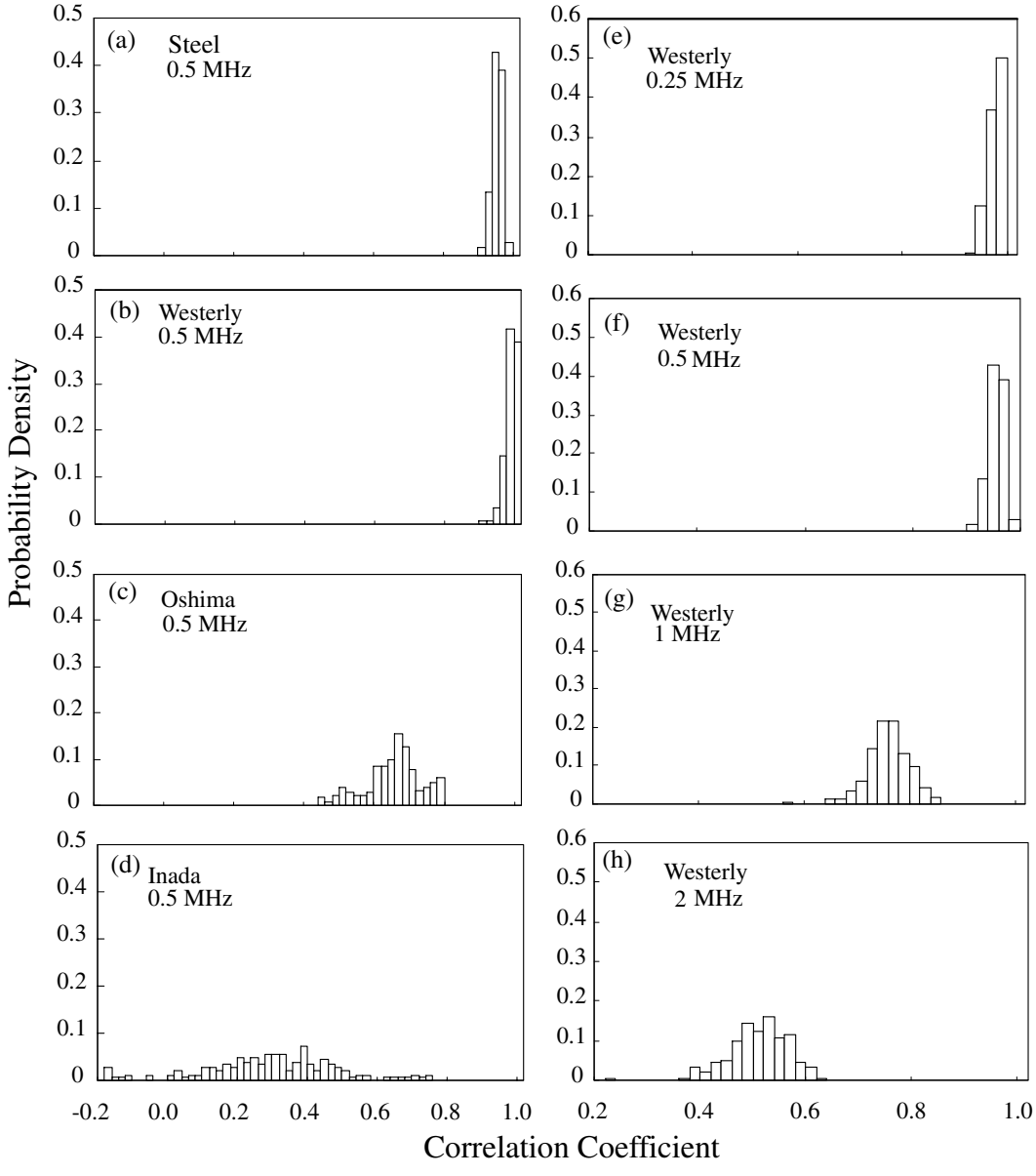

Figure 9. Probability density distribution of correlation coefficient $C_O(i)$ between coherent and observed waveforms for different heterogeneous media: (a) steel, (b) Westerly, (c) Oshima, (d) Inada; and for different frequencies: (e) 0.25, (f) 0.5, (g) 1, (h) 2 MHz in Westerly granite.

and 0.5 MHz sources, the energy of scattered wave is small and the partition pattern is almost uniform with respect to the lapse time. However, the energy of the scattered wave is greater for 1 and 2 MHz sources. For the 1 MHz source, the scattered wave is strongly excited and soon decays after the *P* phase. After the *P* phase, the energy partition shows a broad and weak peak around the *S* phase, and decays gradually with increasing lapse time. For the 2 MHz source, scattered energy is even larger than that of the 1 MHz source. The energy partition of the scattered wave for the 2 MHz source shows a similar pattern to that for the 1 MHz source. The rate of the energy decay after the *S* phase is slightly larger than the 1 MHz scattered wave.

4.5 Fluctuation of arrival times and *P*-phase energy

Distributions of the *P*-wave arrival times are shown in Fig. 12. The histograms of arrival time are converted to a probability density and fitted to the Gaussian probability density function:

$$F(\tau) = \frac{1}{\sqrt{2\pi}\sigma_T} \exp\left[-\frac{(\tau-\mu)^2}{2\sigma_T^2}\right] \quad (12)$$

where τ, μ and σ_T are the traveltime, its average value and the standard deviation of arrival time fluctuation, respectively.

Actually, the observed distributions are not symmetric and are somewhat skewed. It is not correct to fit the distribution to the Gaussian-type distribution. However, to depict the effect of heterogeneity on arrival time, it is still useful to calculate the variance of Gaussian distribution. The variance of arrival time distribution increases from steel, Westerly, Oshima and to Inada, indicating that the arrival-time fluctuation becomes larger with increasing scale of heterogeneity.

We calculated energy fluctuation of the *P*-phase for studying the statistical distribution because this phase is clear for all experiments. The *P*-wave energy was estimated in the window

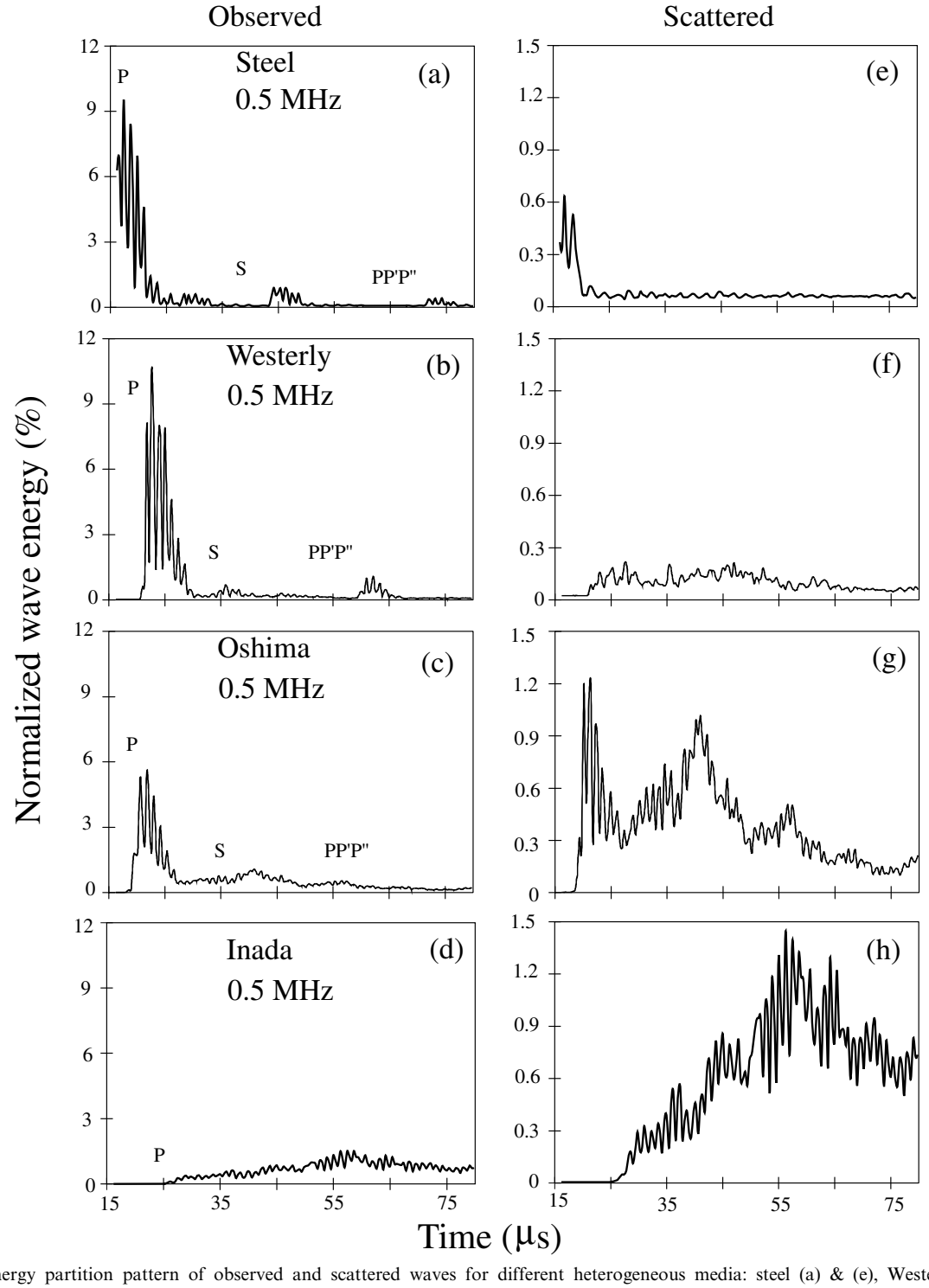

Figure 10. Energy partition pattern of observed and scattered waves for different heterogeneous media: steel (a) & (e), Westerly (b) & (f), Oshima (c) & (g) and Inada (d) & (h).

containing the first cycle of the wave. The window length for calculating *P*-phase energy is 4 μs marked by a rectangle on the waveform (Fig. 5 a), for example. We consider the statistical distributions of the log of the *P*-phase energy (the log-energy). Distributions of the log-energy are shown in Fig. 13. The Gaussian distribution is also fitted to the observed distribution. The variance of the distribution of log-energy increases with increasing scale length of heterogeneity, and also with increasing source frequency in Westerly.

5 DISCUSSION

5.1 Scaling law of seismic waves

Before discussing the present experimental results, we first consider the scaling law of seismic waves. Employing the scaling law of elastic waves, we can describe wave propagation in random heterogeneous media through the parameters ka and kL, where k is the wave number, a is the characteristic scale

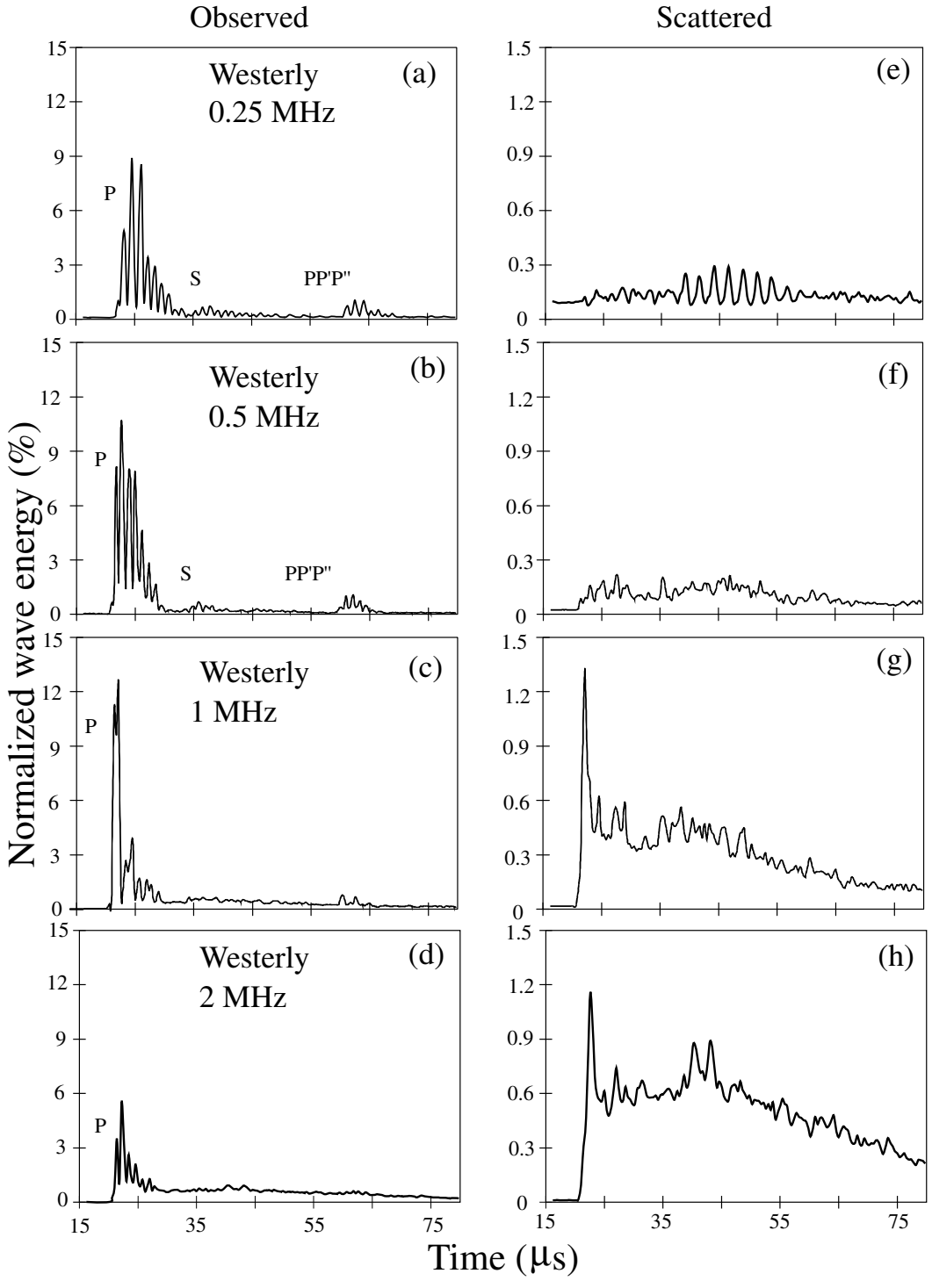

Figure 11. Energy partition pattern of observed and scattered waves for different frequencies in Westerly granite: 0.25 MHz (a) & (e), 0.5 MHz (b) & (f), 1 MHz (c) & (g) and 2 MHz (d) & (h).

length of heterogeneity, and L is the travel distance of the wave. The wave number k is given by $2\pi f/V$, where f is the wave frequency and V is the phase velocity. We measured the phase velocity of three granitic rocks by traveltimes of the direct P and S waves, and the velocity values are almost the same as those reported previously (Press 1966; Mogi 1962; Sano *et al.* 1992).

For 0.5 MHz P wave, we obtain $ka = 0.14$, 0.30 and 0.76 corresponding to Westerly, Oshima and Inada, respectively. For S wave, ka is about 1.7 times larger than that of P wave, if we assume the same a for the S-wave fluctuation. The present source–receiver configuration gives kL about 30–700 for the direct P and $P'PP''$ phases with the frequencies from 0.25 to

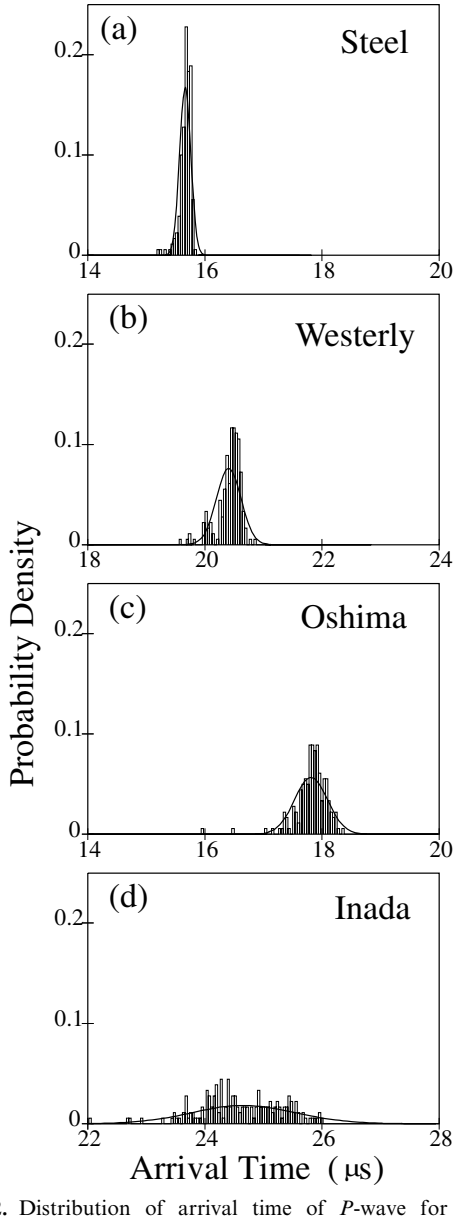

Figure 12. Distribution of arrival time of *P*-wave for (a) steel, (b) Westerly, (c) Oshima and (d) Inada granites. The histogram represents the observed distribution and the solid curve represents the fitted Gaussian probability density function.

2 MHZ. For the 0.25–2 MHz source frequency in Westerly, *ka* of *P* wave ranges from 0.07 to 0.56. Fig. 14 shows a *ka*–*kL* diagram of scattering problem together with methods for studying seismic waves (Aki & Richards, 1980). The hatched area in the *ka*-*kL* diagram includes all values of *ka* and *kL* for *P* and *S* waves in the present experiments. The thick solid and dashed lines in that area indicates the *ka*–*kL* relationships for *P* and $PP'P''$ phases of the three-rock experiments, and $PP'P''$ phase of the four-frequency experiments, respectively.

The present experiments range from the area of equivalent homogeneous body to the wave theories for random media in the *ka*–*kL* diagram. When *ka* or *kL* becomes large, the wave field becomes more complex and wave theories should be applied.

5.2 Relationship between waveform parameters and heterogeneity

The statistics of the waveform parameters for three-rock experiments are shown in Table 3: the average of cross correlation between observed and coherent waves at the stations, $\overline{C}_O$; and the standard deviations of the C_O distribution, σ_C; the arrival time distribution, σ_T; and the log-energy distribution, σ_E; together with the *a* and *ka* values. Table 4 shows the same statistical parameters except for arrival time for the frequency experiments, together with source frequency *f* and *ka*. The average cross correlations between coherent and observed waves are plotted against the scale length of heterogeneity or *ka* in Fig. 15(a), for the three-rock experiments and in Fig. 16(a) for the frequency experiments. In the three-rock experiments, the C_O of steel and Westerly are almost same, but it decreases in Oshima and more in Inada. The standard deviations of σ_C, σ_T and σ_E show similar values between steel and Westerly, and increase in Oshima and more in Inada. In the frequency experiments, C_O of 0.25 and 0.5 MHz are almost the same but they change considerably when the frequency exceeds 0.5 MHz. σ_C and σ_E show the change at 1 MHz; they show similar values for 0.25 and 0.5 MHz and increase at 1 MHz and more at 2 MHz. In both three-rock and different-frequency experiments, the increasing or decreasing trends of statistical parameters change at $ka(P) \sim 0.2$, where $ka(P)$ is the *ka* for *P* wave, except for the standard deviation of the arrival time distribution of the *P*-wave, whose trend changes when $ka(P)$ exceeds 0.3.

5.3 Scattered waves in the exponential type ACF

Figs 10(g,h) and Figs 11(g,h) show that a large amount of energy is scattered in the later portion of waveforms when $ka(P)$ exceeds 0.2–0.3. When $ka(P)$ exceeds these values, the scattered waves are considered to be produced by multiple scattering of *P* and *S* waves. The scattered waves are also produced by wide-angle scattering of *S* waves because most of scattered energy appears after the *S*-phase arrival and is stronger than the observed *S* phase in the waveform. Figs 7(a–h) show that waveform correlations of *S* and $PP'P''$ phases decay more rapidly than *P* phase. Since *P* phase appears as the first phase of waveform and its fluctuation is affected only by forward scattering, *P* phase is not strongly fluctuated and shows a good spatial correlation compared to *S* and $PP'P''$ phases, which contain more scattered waves caused by multiple and wide-angle scattering.

The rapid increase of waveform fluctuation at $ka\,(P) \sim 0.2$–0.3 may be attributed to the exponential-type ACFs in granitic rocks. Obara & Sato (1995) studied *S*-wave broadening in different heterogeneities. They generalized the ACF of heterogeneity and compared envelope formation in different heterogeneities expressed by the Gaussian type and the exponential type as the two extreme cases. Their results show that envelopes of *S* wave are more sensitive to frequency when ACF of heterogeneity is close to the exponential function. The large scattered energy after the *S* phase in Fig. 10(g) and Figs 11(g–h) agree with their results. Compared to the Gaussian ACF, the exponential ACF has the higher intensity in the wavelength larger than *a* and the lower intensity in the wavelength smaller than *a*. The abrupt changes of statistical parameters in waveform at around $ka(P) \sim 0.2$–0.3 are presumed to be a characteristic feature for the heterogeneities described by the exponential-type ACF.

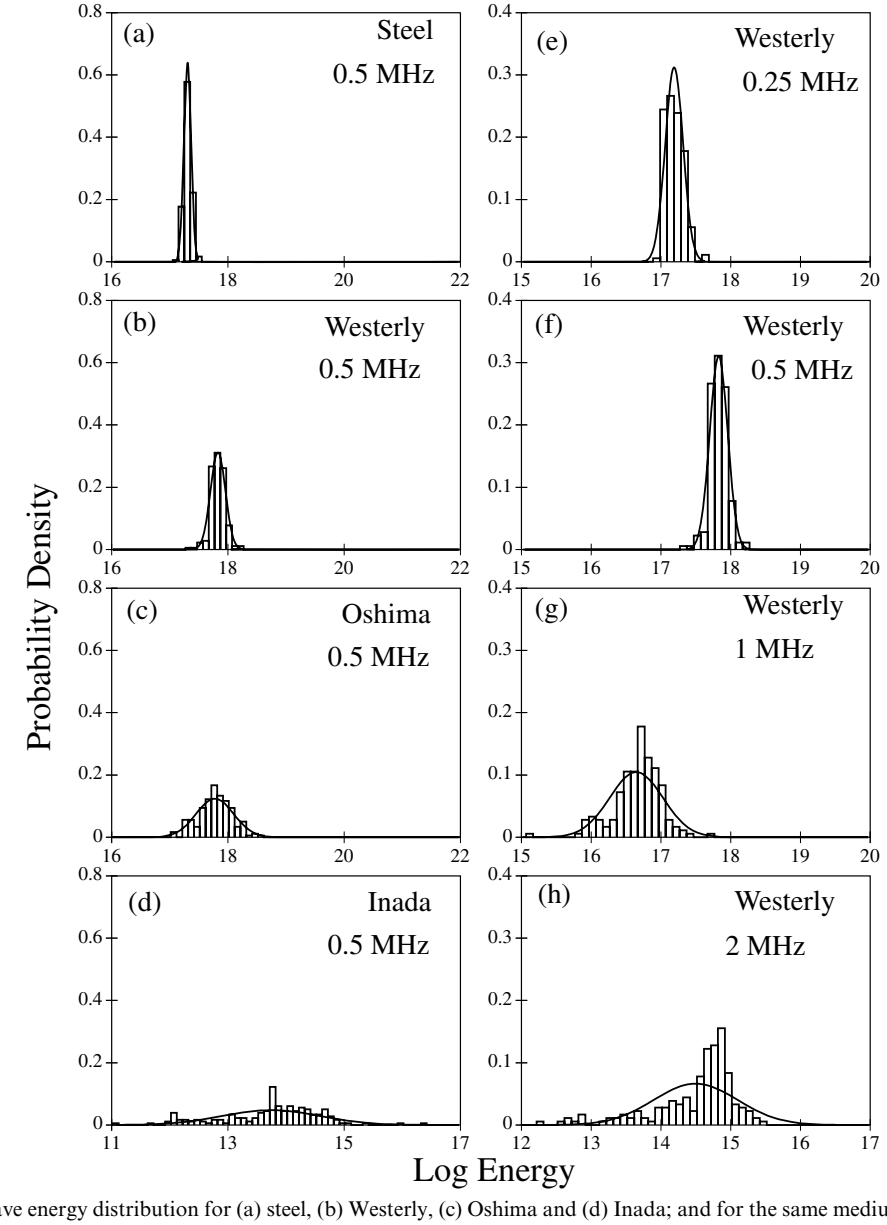

Figure 13. Log of *P*-wave energy distribution for (a) steel, (b) Westerly, (c) Oshima and (d) Inada; and for the same medium (Westerly granite) with different source frequencies: (e) 0.25, (f) 0.5, (g) 1 and (h) 2 MHz. The histogram represents the observed distribution and the solid curve represents the fitted Gaussian probability density function.

5.4 Wave coherence in seismic imaging as a function of *ka*

There have been many studies about wave coherence in exploration geophysics (eg. Yilmaz 1988; Sheriff 1991). However, most data processing methods are based on ray theory that is valid only in a limited range of the *ka–kL* diagram. Ray theory is applicable when the scale of the long-wavelength heterogeneity (target structure) is much larger than the scale of the short-wavelength random heterogeneity. This case corresponds to the equivalent homogeneous body for the short-wavelength heterogeneity in the *ka–kL* diagram. Ray theory predicts the phase in a seismic wave uniquely from the travel distance and traveltime, and the signal phases are detected by phase correlations. However, when the scale of the short-wavelength random heterogeneity becomes large and the scale difference between two heterogeneities becomes small, the signal phases from the long-wavelength heterogeneity are masked by the scattered waves generated from the short-wavelength heterogeneity. On the basis of the present experimental results, we now discuss some problems of identifying the signal phases in seismic wave.

We consider the case of detecting the $PP'P''$ signals in the waveform, for example. When we estimate the block thickness (the target structure) from the $PP'P''$ signal in waveforms, the characteristic scale a of the long-wavelength heterogeneity is around 80–90 mm (block thickness), and the corresponding $ka(P)$ is about 30–200 for 0.25–2 MHz source frequencies. For the $PP'P''$ phase, the travel distance is three times the block thickness, and kL for P wave, $kL(P)$, is 95-750. This range is shown as a hatched zone in Fig. 14. The *ka–kL* relationship for the $PP'P''$ phase is shown as a dashed line in Fig. 14.

Our purpose is to discriminate the wave signal associated with $ka(P) = 30$–200 from the waveform containing the scattered

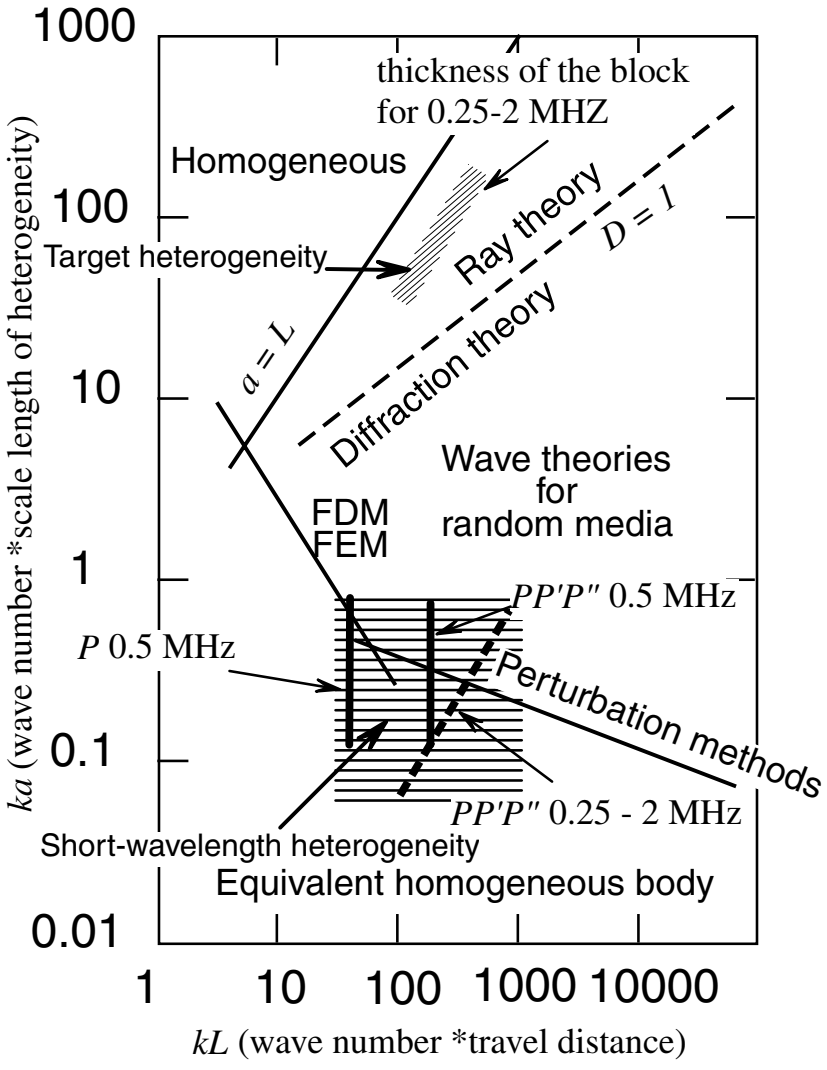

Figure 14. A $ka-kL$ diagram showing scattering problems and applicable methods of seismology. The parameter D is called as the wave number defined by the square of the ratio of the first fresnel zone L_F to the scale length of heterogeneity, (L_F^2/a^2, or $4L/(a^2k)$) for the plane wave. The present experiments are shown by a hatched region and lines. The heterogeneity scale corresponding to the block thickness is in the region of ray-theoretical approach.

wave associated with the short-wavelength random heterogeneity corresponding to $ka(P)=0.07$–0.76. When ka is small, the medium can be regarded as an equivalent homogeneous medium. In this case, we can use ray theory to distinguish the boundary between equivalent homogeneous media. This corresponds to the case of Westerly with source frequencies of 0.25 and 0.5 MHz, where the $PP'P''$ phase is clearly discernible and shows high correlation values even for large array distances (Fig. 7). On the other hand, when ka increases and becomes close to the region of scattered wave theories, the wave field is strongly affected by scattered waves and $PP'P''$ phase is not discernible. This corresponds to the case of Westerly with 1 MHz source frequency, or the case of Oshima and Inada with 0.5 MHz source frequency, where the $PP'P''$ phase cannot be seen and phase correlation disappears even at short distances. The boundary between the two cases locates at $ka(P)\sim 0.2$–0.3. This gives an important knowledge that equivalent homogeneous medium approximation breaks at $ka(P)\sim 0.2$–0.3. The breaking point well corresponds to the changes of the timeshift-fluctuation trend (a similar meaning of arrival time fluctuation) calculated from scattering theory for the 2-D and the 3-D cases (Spetzler *et al.* 2001). Breaking of the equivalent homogeneous medium approximation suggests difficulties in discriminating signal phases of observed waves and also difficulties in application of ray theory to describe wave propagation in heterogeneous media. If we use too much high frequency for source signal, we never obtain the target heterogeneity because $ka(P)$ for the short-wavelength exceeds 0.2–0.3. If we use too much low frequency for the source signal, $ka(P)$ becomes small and scattered wave is not strong, but $ka(P)$ of the target heterogeneity is also small and may be out from the area of ray theory. In this case, we have to consider diffraction waves from the heterogeneity of which scale length is close to the target heterogeneity. We must consider the trade-off of ka values between target heterogeneity and the short-wavelength random heterogeneity when selecting seismic wave frequencies applicable to ray theory. Increasing the station density of seismic array or increasing the number of seismic ray paths cannot improve the resolution problem of seismic imaging because wave coherence disappears at very short distances when scattered wave is strong, as suggested in the present experiments.

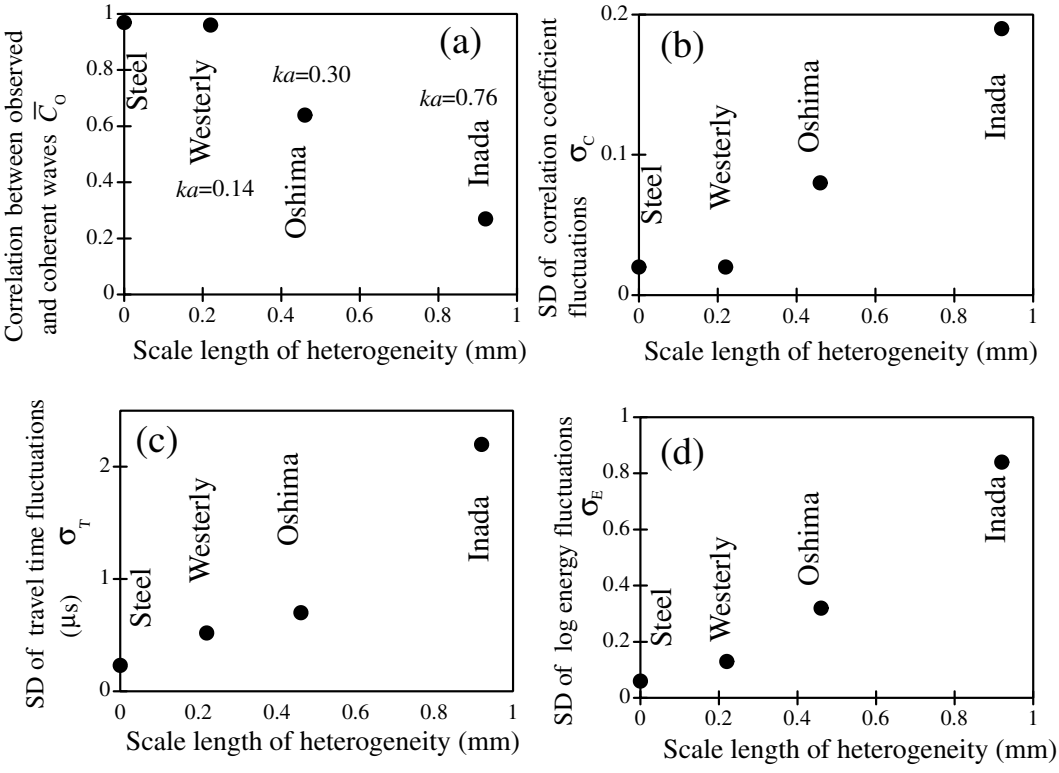

Figure 15. Relationships between statistical parameters of waveform fluctuation and the characteristic length of heterogeneity of the medium: (a) correlation coefficient between coherent and observed waves $\overline{C}_O$; (b) standard deviation of fluctuation of correlation coefficient σ_C; (c) standard deviation of the fluctuation of *P*-wave arrival time σ_T; and (d) standard deviation of fluctuations of log of *P*-wave energy σ_E. *ka* is shown in the figure.

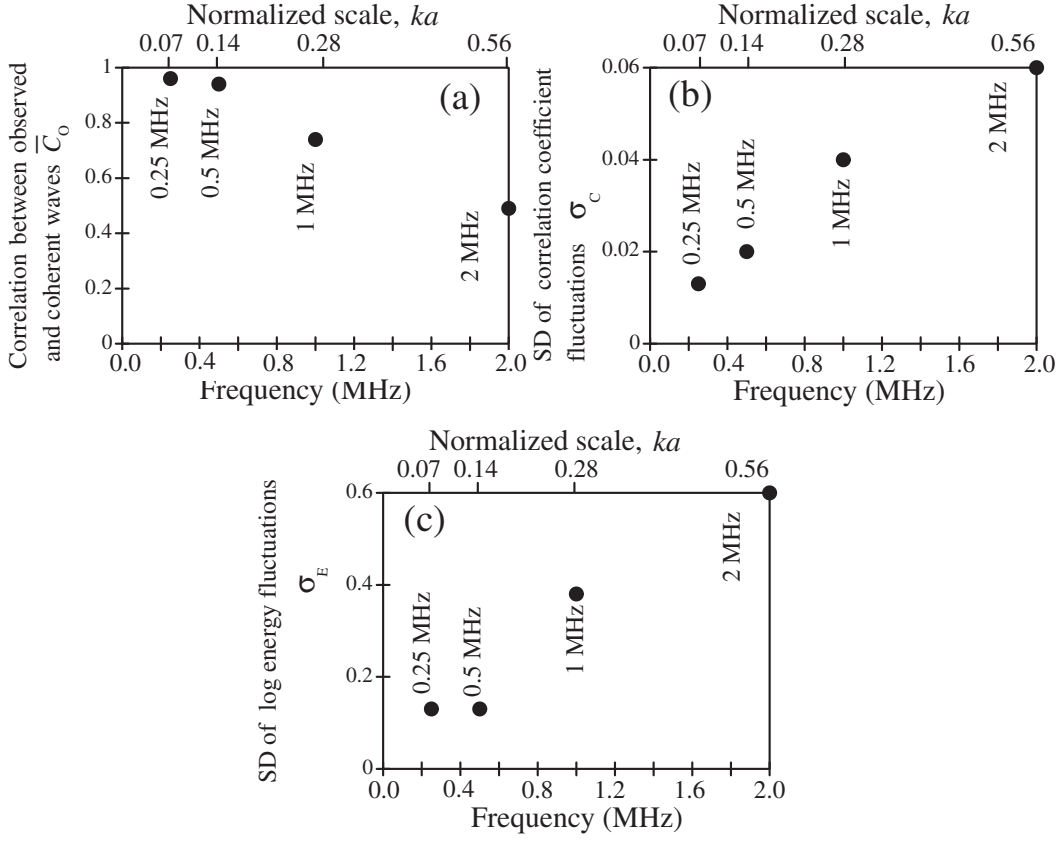

Figure 16. Relationships between statistical parameters of waveform fluctuation and the source frequency or normalized scale parameter *ka*: (a) correlation coefficient between coherent and observed waves $\overline{C}_O$; (b) standard deviation of fluctuations of correlation coefficient σ_C; and (c) standard deviation of fluctuations of the log of *P*-wave energy σ_E.

6 CONCLUSIONS

It is now recognized that the noise in a seismic wave is not an independent time-series from the original seismic wave but a signal-induced wave mostly consisting of scattered waves (Scales & Snieder 1998). This is important for seismic data processing but not well recognized in the field of seismology and seismic explorations. For example, when we simulate seismic data, we add noise in the original seismic wave. In this case, the noise should be a signal-induced wave, and it must be calculated from the interaction between the short-wavelength heterogeneity and the original wave.

Using 2-D numerical simulations for acoustic wave, Gibson & Levander (1988) studied the effect of signal-induced noise on conventional seismic data processing techniques. They examined the effect of two kinds of noises on conventional seismic data processing: the noise produced from the near-surface topography and the noise produced from the random heterogeneity of the deeper layer. They found that these two kinds of noise affect the signal waves in different ways and the two effects can be distinguished from each other. We demonstrated an example of noise generated from random heterogeneity by means of physical model experiments. In physical model experiments using rock samples, we can model 3-D heterogeneous systems and S wave scattering. As suggested in our study of energy partition with respect to lapse time, the S wave scattering is strong and affects the later portion of the waveform. The effects of the S wave are not well studied by numerical experiments because of its complexity. However, it is important to examine the effects of S wave scattering, when we study seismic wave propagation in crystalline rocks.

On the basis of well-log data, Goff & Holliger (1999) revealed that spectral density of velocity fluctuations in crystalline crust is a band-limited fractal characterized by $1/f$ decay in the short-wave fluctuations and more steeper decay around the short-wave limit. Similar results are also reported (Wu *et al.* 1994; Shiomi *et al.* 1997). The fractal nature of velocity fluctuation causes a serious problem because it implies that there is no characteristic scale length in the heterogeneity of the crust, and seismic waves will interact with heterogeneity in the same way for all wavelengths. This results in difficulties in determining underground structure because the resolution of heterogeneity is identical for all scale lengths. However, many successful results of exploration seismology suggest a flat spectral density or spectral peaks at the long-wavelength limit. The present experiments suggest that the transition from the equivalent homogeneous medium to the scattering medium exists at $ka(P) \sim 0.2$–0.3 for exponential heterogeneous media of $\varepsilon \sim 10$ per cent. This ε is larger than the intensity of slowness fluctuation in the earth's crust, which is recently reported as 1–8 per cent (Yoshimoto *et al.* 1997; Rothert and Ritter 2000; Hock *et al.* 2000; Line *et al.* 1998a; Roth 1997). Present experiments may exaggerate the effect of random heterogeneity on seismic waves, and the critical $ka(P)$ value could be less in field observation. It is thus important to know more about the spectral density and intensity of the crustal heterogeneity.

Recently, huge computers have been employed for numerical simulation of seismic waves in 3-D media, but it is still difficult to calculate signal-induced scattered waves in 3-D random heterogeneous media. Therefore, physical model experiments are still valuable for studying data processing techniques in seismology and seismic exploration. Since LDV can provide full waveform in laboratory-scale physical model experiments with flat response over appropriate frequencies, we can study seismic waves in heterogeneous media more accurately by employing LDV as a sensor for elastic waves.

ACKNOWLEDGMENTS

The authors thank Prof. H. Sato, Drs. R. Kranz, M. Hoshiba and J. Spetzler for their useful discussions and comments on the manuscript. They also thank to Dr. X. Lei for the software of waveform analysis and Ms. Y. Nakashima for assisting experiments. This study is supported from the AIST's special research budget for new energy development. CS is grateful to the Science and Technology Agency of Japan for giving an opportunity to carry out this study. CS is thankful to Prof. V. S. Ramamurthy, Secretary, Department of Science and Technology, Government of India for according necessary leave to carry out this study at Geological Survey of Japan, and to Dr. G. D. Gupta, Head Seismology Division, DST, India for his encouragement.

REFERENCES

Aki, K., 1973, Scattering of *P* waves under the Montana Lasa, *J. geophys. Res.,* **78,** 1334–1346.

Aki, K., Chouet, B., 1975, Origin of coda waves: Source, attenuation and scattering effects, *J. geophys. Res.,* **80,** 3322–3342.

Aki, K. & Richards, P.G., 1980, *Quantitative Seismology,* W. H. Freeman & Co., San Francisco.

Alekesandrov, K.S. & Ryzhova, T.V., 1961. The elastic properties of rock-forming minerals, II: layered silicates, *Izv. Acad. Sci. USSR, Geophys. Ser.,* **2,** 186–189.

Campillo, M., Margerin, L., 1999, Seismic wave diffusion in the earth lithosphere, in *Diffuse waves in complex media,* ed. Fopuque J.P., 383–404.

Canas, J.A., Ugalde, A., Pujades, L.G., Carracede, J.C., Soler, V., Blanco, M.J., 1998, Intrinsic and scattering attenuation in the Canary Islands, *J. geophys. Res.,* **103,** 15 037–15 050.

Derode, A. & Fink, M., 1997, Partial coherence of transient ultrasonic fields in anisotropic random media: Application to coherent echo detection, *J. accoust. Soc. Am.,* **101,** 690–704.

Derode, A. & Fink, M., 1998, correlation length of ultrasonic speckle in anisotropic random media: Application to coherent echo detection, *J. accoust. Soc. Am.,* **103,** 73–82.

Dubendorff, B. & Menke, W., 1986, Time-domain apparent-attenuation operators for compressional and shear waves: Experiment versus single-scattering theory, *J. geophys. Res.,* **91,** 14 023–14 032.

Fehler, M., Hoshiba, M., Sato, H., Obara, K., 1992, Separation of scattering and intrinsic attenuation for the Kanto-Tokai region, Japan, using measurements of S-wave energy versus hypocentral distance, *Geophys. J. Int.,* **108,** 787–800.

Flatte, S.M. & Wu, R.S., 1988, Small-scale structure in the lithosphere and asthenosphere deduced from arrival time and amplitude fluctuations at NORSAR, *J. geophys. Res.,* **93,** 6601–6614.

Frankel, H. & Clayton, R.W., 1986, Finite difference simulation of seismic scattering: Implications for the propagation of short-period seismic waves in the crust and models of crustal heterogeneity, *J. geophys. Res.,* **91,** 6465–6489.

Frankel, A., Wennerberg, L., 1987, Energy-flux model of seismic coda: separation of scattering and intrinsic attenuation, *Bull. seism. Soc. Am.,* **77,** 1223–1251.

Fukushima, Y., 2000, Laboratory study on scattering characteristics of shear waves in rock samples, *M.Sc. Thesis* Tohoku University, Japan.

Gibson, B.S. & Levander, A.R., 1988, Modeling and processing of scattered waves in seismic reflection surveys, *Geophysics,* **53,** 466–478.

Goff, J.A. & Holliger, K., *et al.*, 1999, Nature and origin of upper crustal seismic velocity fluctuations and associated scaling properties: Combined stochastic analyses of KTB velocity and lithology logs, *J. geophys. Res.,* **104,** 13 169–13 182.

Hock, S., Korn, M., Group, T.T.W., 2000, Random heterogeneity of the lithsphere across the Trans European Suture Zone, *Geophys. J. Int.,* **141,** 57–70.

Holliger, K. & Levander, A., 1992, A stochastic view of lower crustal fabric based on evidence from the Ivrea Zone, *Geophys. Res. Lett.,* **19,** 1153–1156.

Holliger, K. & Levander, A., 1994, Seismic structure of gneissic/granitic upper crust: geological and petrophysical evidence from the Strone-Ceneri Zone (northern Italy) and implications for crustal seismic exploration, *Geophys. J. Int.,* **119,** 497–510.

Horike, M., Takeuchi, Y., 2000, Possibility of spatial variation of high-frequency seismic motions due to random-velocity fluctuation of sediments, *Bull. seism. Soc. Am.,* **90,** 48–65.

Hoshiba, M., 1993, Separation of scattering attenuation and intrinsic absorption in Japan using the multiple lapse time window analysis, *J. geophys. Res.,* **98,** 15 809–15 824.

Hoshiba, M., 2000, Large fluctuation of wave amplitude produced by small fluctuation of velocity structure, *Phys. Earth Planet. Inter.,* **120,** 201–217.

Ishimaru, A., 1975, Correlation functions of a wave in a random distribution of stationary and moving scatterers, *Radio Sci.,* **10,** 45–52.

Jannaud, L.R., Adler, P.M., Jacquin, C.G., 1991, Frequency dependence of the Q factor in random media, *J. geophys. Res.,* **96,** 18 233–18 243.

Kinney, W.A. & Clay, C.S., 1984, The spatial coherence of sound scattered from a wind driven surface: Comparison between experiment, Eckart theory, and the facet-ensemble method, *J. acoust. Soc. Am.,* **75,** 145–148.

Kitagawa, G., Akaike, H., 1978, Procedeure for the modeling of non-stationary time series, *Annals Inst. Statis. Math.,* **30,** 351–363.

Knopoff, L., Hudson, J.A., 1967, Frequency dependence of amplitudes of scattered elastic waves, *J. acoust. Soc. Am.,* **42,** 18–20.

Korn, M., 1997, Modelling of the teleseismic P coda envelope: depth dependent scattering and deterministic structure, *Phys. Earth Planet. Inter.,* **104,** 23–36.

Korn, M., 1990, A modified energy flux model for lithospheric scattering of teleseismic body waves, *Geophys. J. Int.,* **102,** 165–175.

Line, C.E.R., Hobbs, R.W., Hudson, J.A., Snyder, D.B., 1998a, Statistical inversion of controlled source seismic data using parabolic wave scattering theory, *Geophys. J. Int.,* **132,** 61–78.

Line, C.E.R., Hobbs, R.W., Snyder, D.B., 1998b, Estimates of upper-crustal heterogeneity in the Baltic Shield from seismic scattering and borehole logs, *Tectonophysics,* **286,** 171–183.

Lynnes, C.S & Lay, T., *et al.*, 1990, Effects of lateral velocity heterogeneity under the Nevada Test Site on short-period P wave amplitudes and travel times, *Pure App. Geophys.,* **132,** 245–267.

Menke, W., 1999, Using waveform similarity to constrain earthquake locations, *Bull. seism. Soc. Am.,* **89,** 1143–1146.

Menke, W., Lerner-Lam, A.L., Dubendorff, B., Pacheco, J., 1990, Polarization and coherence of 5 to 30 Hz seismic wave fields at a hard-rock site and their relevance to velocity heterogeneities in the crust, *Bull. seism. Soc. Am.,* **80,** 430–449.

Menke, W., Witte, D., Chen, R., 1985, Laboratory test of apparent attenuation formulas, *Bull. seism. Soc. Am.,* **75,** 1383–1393.

Menke, W., Levin, V., Sethi, R., 1995, Seismic attenuation in the crust at the mid-Atlantic plate boundary in south-west Iceland, *Geophys. J. Int.,* **122,** 175–182.

Mogi, K., 1962, Study of elastic shocks caused by the fracture of heterogeneous materials and its relations to earthquake phenomena, *Bull. Earthq. Res. Inst.,* **40,** 125–173.

Muller, G., Roth, M., Korn, M., 1992, Seismic-wave travel times in random media, *Geophys. J. Int.,* **110,** 29–41.

Nishizawa, O., Satoh, T., Lei, X. & Kuwahara, Y., 1997, Laboratory studies of seismic wave propagation in inhomogeneous media using a laser Doppler vibrometer, *Bull. seism. Soc. Am.,* **87,** 809–823.

Nishizawa, O., Satoh, T., Lei, X., 1998, Detection of shear wave in ultrasonic range by using laser Doppler vibrometer, *Rev. Scient. Instr.,* **69,** 2572–2573.

Obara, K. & Sato, H., 1995, Regional differences of random inhomogeneities around the volcanic front in the Kanto-Tokai area, Japan, revealed from the broadening of S wave seismogram envelopes, *J. geophys. Res.,* **100,** 2103–2121.

Parra, J.O., Hackert, C.L., Ababou, R., Sablik, M.J., 1999, Dispersion and attenuation of accoustic waves in randomly heterogeneous media, *J. app. Geophys.,* **42,** 99–115.

Pechmann, J.C., Kanamori, H., 1982, Waveforms and spectra of preshocks and aftershocks of the 1979 Imperial Valley, California earthquake: Evidence for fault heterogeneity?, *J. geophys. Res.,* **87,** 10,579–10,597.

Press, F., 1966, Seismic velocities, in *Handbook of Physical Constants,* ed. Clark, Jr., S.P., 195–221, Geological Society of America, New York.

Pullammanappallil, S, Levander, A., Larkin, S.P., 1997, Estimation of crustal stochastic parameters from seismic exploration data, *J. Geophys., Res.,* **102,** 15 269–15 286.

Roth, M., 1997, Statistical interpretation of travel time fluctuations, *Phys. Earth Planet. Inter.,* **104,** 213–228.

Rothert, E. & Ritter, J.R.R., 2000, Small-scale heterogeneities below the Gräfenberg array, Germany from seismic wavefield fluctuations of Hindu Kush events, *Geophys. J. Int.,* **140,** 175–184.

Sano, O., Kudo, Y., Mizuta, Y., 1992. Experimental determination of elasitc constants of Oshima granite, Barre granite, and Chelmsford granite, *J. geophys. Res.,* **97,** 3367–3379.

Sato, H., 1984, Attenuation and envelope formation of three component seismograms of small local earthquakes in randomly inhomogeneous lithosphere, *J. geophys. Res.,* **89,** 1221–1241.

Sato, H. & Fehler, M., 1998, Seismic wave propagation and scattering in the heterogeneous earth, AIP Series in Modern Acoustic and Signal processing, Springer-Verlag, New York, 1–308.

Scales, J.A. & Snieder, R., 1998, What is noise?, *Geophysics,* **63,** 1122–1124.

Sheriff, R.E., 1991, Encyclopedic dictionary of exploration geophysics, *Soc. Expl. Geophys.,* Tulsa.

Shiomi, K., Sato, H. & Ohtake, M., 1997, Broad-band power-law spectra of well-log data in Japan, *Geophys. J. Int.,* **130,** 57–64.

Sivaji, C., Nishizawa, O., Fukushima, Y., 2001, Relationship between fluctuations of arrival time & energy of seismic waves and scale length of heterogeneity: An inference from experimental study, *Bull. seism. Soc. Am.,* **91,** 292–303.

Spetzler, J. & Snieder, R., 2001, The effect of small-scale heterogeneity on the arrival time of waves, *Geophys. J. Int.,* **145,** 786–796.

Spetzler, J., Sivaji, C., Nishizawa, O. & Fukushima, Y., 2002, A test of ray theory and scattering theory based on a loboratory experiment using ultrasonic waves and numerical simulations by finete-difference method, *Geophys. J. Int.* **148,** 165–178.

Takanami, T. & Kitagawa, G., 1991, Estimation of the arrival times of seismic waves by multivariate time series model, *Annals Inst. Stat. Math.,* **43,** 403–433.

Tang, X.M., Zhu, Z., Toksöoz, M.N., 1994, Radiation patterns of compressional and shear transducers at the surface of an elastic half-space: *J. acoust. Soc. Am.,* **95,** 71–76.

Thorbjarnadottir, B.S., Pechmann, J.C., 1987, Constraints on relative earthquake locations from cross-correlation of waveforms, *Bull. seism. Soc. Am.,* **77,** 1626–1634.

Varadan, V.K., Ma, Y., Varadan, V.V., 1989, Scattering and attenuation of elastic waves in random media, *Pure App. Geophys.,* **131,** 577–603.

Wu, R.S., Xu, Z. & Li, X.P., 1994, Heterogeneity spectrum and scale-anisotropy in the upper crust revealed by the German Continental Deep-Drilling (KTB) Holes, *Geophys. Res. Lett.,* **21,** 911–914.

Yilmaz, O., 1988, Seismic Data Processing, *Soc. Expl. Geophys.,* Tulsa, USA.

Yoshimoto, K., Sato, H & Ohtake, M., 1993, Frequency-dependent attenuation of P and S waves in the Kanto area, Japan, based on the coda-normalization method, *Geophys. J. Int.,* **114,** 165–174.

Yoshimoto, K., Sato, H & Ohtake, M., 1997, Short-wavelength crustal heterogeneities in the Nikko area, Central Japan, revealed from the three-component seismogram envelope analysis, *Phys. Earth. Planet. Int.,* **104,** 63–73.